A BOUNDED ARTIFICIAL VISCOSITY MODEL FOR THE NUMERICAL SIMULATION OF TURBULENT FLOWS

JEFF BORGGAARD *, TRAIAN ILIESCU †, AND JOHN PAUL ROOP ‡

Abstract. In this paper, we present a rigorous numerical analysis for a bounded artificial viscosity model for the numerical simulation of turbulent flows. In practice, the commonly used Smagorinsky model $\left(\tau = (c_s\delta)^2|\nabla^s u|\nabla^s u\right)$ is overly dissipative, and yields unphysical results. To date, several methods for "clipping" the Smagorinsy viscosity have proven useful in improving the physical characteristics of the simulated flow. However, such heuristic strategies rely strongly upon *a priori* knowledge of the flow regime. The bounded artificial viscosity model, as introduced in [15], relies on a highly nonlinear, but strongly monotone and smooth, semilinear elliptic form for the artificial viscosity. For such a bounded model, we have introduced a variational computational strategy, provided finite element error convergence estimates, and included several computational examples indicating its improvement over the overly diffusive Smagorinsky model.

Key words. Large eddy simulation, turbulence, artificial viscosity, Smagorinsky model

AMS subject classifications. 15A15, 15A09, 15A23

1. Introduction. In this paper, we present analysis and numerical computations for a bounded artificial viscosity model for the numerical simulation of viscous incompressible flow problems. We consider models for the turbulent viscosity coefficient which depend on bounded, smooth, increasing functions (e.g. that depicted in Figure 1) of the magnitude of the deformation tensor. As the Smagorinsky eddy viscosity model is widely known to be overly dissipative (**References here!!!**), strategies must be developed by which the eddy viscosity is reduced in particular portions of the flow regime. We argue that the bounded artificial viscosity model can be used as a viable alternative to other highly successful damping procedures, which are tailored to particular flow regimes about which much is known.

Turbulence is central to many important applications such as global change estimation, improving the energy efficiency of engines, controlling dispersal of contaminants, and designing biomedical devices. It is absolutely fundamental to understanding physical processes of geophysics, combustion, forces of fluids upon elastic bodies, drag, lift and mixing. To this end, much attention has been paid to the problem of not only accurately simulating turbulent flow, but also to providing reasonable approximations at relatively small computational cost.

Direct numerical simulation of turbulent flows is not feasible for the foreseeable future in many of these applications. Indeed, Kolmogorov's 1941 theory (K-41) of homogeneous, isotropic turbulence predicts that small scales exist down to $O(Re^{-3/4})$, where $Re > 0$ is the Reynolds number. Thus, in order to capture all scales on a mesh,

*Department of Mathematics, Virginia Polytechnic Institute and State University, 528 McBryde Hall, Blacksburg, VA 24061, U.S.A., (borggaard@vt.edu); partially supported by AFOSR grants F49620-00-1-0299, F49620-03-1-0243, and FA9550-05-1-0449 and NSF grants DMS-0322852 and DMS-0513542.

†Department of Mathematics, Virginia Polytechnic Institute and State University, 456 McBryde Hall, Blacksburg, VA 24061, U.S.A., (iliescu@math.vt.edu); partially supported by AFOSR grants F49620-03-1-0243, and FA9550-05-1-0449 and NSF grants DMS-0209309, DMS-0322852, and DMS-0513542.

‡Department of Mathematics, Virginia Polytechnic Institute and State University, 456 McBryde Hall, Blacksburg, VA 24061, U.S.A., (jroop@math.vt.edu); partially supported by AFOSR grants F49620-03-1-0243, and FA9550-05-1-0449 and NSF grants DMS-0209309, DMS-0322852, and DMS-0513542.

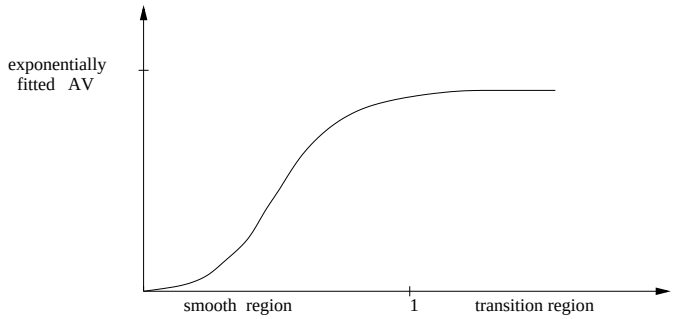

Figure 1: The graph of $a(\cdot)$; the horizontal axis represents $\|h\nabla u^h\|$.

we need a mesh-size $h \sim Re^{-3/4}$, and consequently (in 3D) $N \sim Re^{9/4}$ mesh points.

Large eddy simulation (LES) is one of the most successful approaches in the numerical simulation of turbulent flows. LES seeks to calculate the large, energetic structures (the large eddies) in a turbulent flow. The large structures are defined by convolving the flow variables with a rapidly decaying spatial filter g_δ. To derive equations for $\overline{\boldsymbol{u}}$, the large eddy flow structure, we convolve the NSE with $g_\delta(\mathbf{x})$. The resulting system is not closed, since it involves both $\boldsymbol{u}$ and $\overline{\boldsymbol{u}}$. The tensor $\boldsymbol{\tau}(\boldsymbol{u},\boldsymbol{u}) = \overline{\boldsymbol{u}\,\boldsymbol{u}^T} - \overline{\boldsymbol{u}}\,\overline{\boldsymbol{u}}^T$ is often called the subgrid-scale stress (SGS) tensor. Thus, the closure problem in LES is to model the SGS tensor $\boldsymbol{\tau}(\boldsymbol{u},\boldsymbol{u})$.

Although many approaches to the closure problem for LES prevail in the literature, the simplest and most commonly used among them is the Eddy Viscosity (EV) model. EV models are motivated by the idea that the global effect of the SGS stress tensor $\boldsymbol{\tau}(\boldsymbol{u},\boldsymbol{u})$, in the mean, is to transfer energy from resolved to unresolved scales through inertial interactions. EV models are motivated by K-41 theory and its associated *energy cascade* ([11, 24, 28]). Thus, the action of the SGS stress $\boldsymbol{\tau}$ is thought of as having a dissipative effect on the mean flow[5]. The mathematical realization is the model

$$\nabla\cdot\boldsymbol{\tau}(\boldsymbol{u},\boldsymbol{u}) \approx -\nabla\cdot(\nu_T\nabla^s\overline{\boldsymbol{u}}) + \text{ terms incorporated into } \overline{p},$$

where $\nabla^s\overline{\boldsymbol{u}}$ is the deformation tensor and $\nu_T \geq 0$ is the "turbulent viscosity coefficient". The modeling problem then reduces to determining one parameter: the turbulent viscosity coefficient $\nu_T(\overline{\boldsymbol{u}},\delta)$.

The most common EV model is known in LES as the *Smagorinsky model* in which

$$\nu_T = \nu_{\text{Smag}}(\overline{\boldsymbol{u}},\delta) := (c_s\delta)^2\|\nabla^s\overline{\boldsymbol{u}}\|_F. \tag{1.1}$$

This model was studied in [31] as a nonlinear artificial viscosity in gas dynamics and in [29] for geophysical flow calculations. A complete mathematical theory for partial differential equations involving this term was constructed by Ladyžhenskaya [18, 19]. Lilly [21] showed (under a number of optimistic assumptions) that c_s has a simple, universal value 0.17.

Although the Smagorinsky model is easy to implement, stable, and replicates energy dissipation rates, it is quite inaccurate for many problems. Probably the most common complaint for the Smagorinsky model (1.1) is that it is *too dissipative*. The reason in clearly illustrated in Figure 1: for large values of the velocity deformation tensor, the Smagorinsky model introduces an unbounded amount of artificial viscosity (AV). This behavior in manifest in practical computations of flows displaying large

velocity deformation tensors, such as wall-bounded flows. For example, for turbulent channel flows and pipe flows [24], the Smagorinsky model yields unphysical results. (**MANY references here!!!!**)

Different approaches have been devised to cope with this limitation. One approach is to use a "clipping procedure", in which essentially the computed coefficient ν_T is clipped every time it exceeds a prescribed value. For wall-bounded flows, a straightforward modification of the Smagorinsky model is the van Driest damping [30] which uses the turbulent boundary layer theory to match the velocity profile near the boundary. For stratified flows, one common modification is to use a Ri-dependent model, where Ri is the Richardson number of the flow (**References here!!!**). Other more involved damping procedures are the *dynamic* SGS models introduced by [12], in which c_s is chosen locally in space and time, $c_s = c_s(\mathbf{x}, t)$. Among these is the *Lagrangian dynamic* SGS model of [22, 25]. All of these approaches target the same deficiency of the Smagorinsky model – its overly diffusive character.

In this paper, we consider a *bounded artificial viscosity model* for the numerical simulation of turbulent flows with high velocity deformation tensors. The bounded AV model has a *general* form: it can be used to reduce the overly dissipative nature of the Smagorinsky model without massive *a priori* knowledge of the flow regime. The bounded AV model reads

$$\nu_T = \mu \delta^{\sigma} a(\delta \|\nabla \boldsymbol{u}\|_F) \nabla \boldsymbol{u}, \tag{1.2}$$

where $a(\cdot)$ is a general function whose graph resembles that in Figure 1.

The bounded AV model was proposed in [15] as an alternative to the Smagorinsky model and yielded improved results for convection-dominated convection-diffusion problems. In this paper, we analyze and test the bounded AV model (1.2) in the numerical simulation of incompressible fluid flows.

The paper is organized as follows. In Section 2, we discuss the commonly used eddy viscosity model. We note the benefits and limitations of heuristic procedures in which a "clipping" of the Smagorinsky artificial viscosity is performed, and present (1.2) as a viable alternative to such strategies. In Section 3, we provide the variational setting for which the NSE with (1.2) is solved and introduce the necessary notations. In Section 4, we present some stability results for the variational solution to NSE with (1.2), which are generalizations of Leray's inequality for the usual Navier-Stokes system. In Section 5, we prove an error estimate for the semi-discrete finite element approximation of NSE with (1.2). Finally, in Section 6, we include finite element calculations for NSE with (1.2) which both support the theoretical error estimate of Section 6, and show that the bounded AV model (1.2) better results than the Smagorinsky model (1.1) in the numerical simulation of channel flows. We provide both sequential computations for an academic vortex decay problem and parallel computations for 2D and 3D channel flows, using the Virginia Tech Large Eddy Simulator (ViTLES).

2. Large Eddy Simulation. LES is connected to a natural computational idea: when a computational mesh is so coarse that the problem data and solution sought fluctuate significantly inside each mesh cell, it is only reasonable to replace the problem data by mesh cell averages of that data and for the approximate solution to represent a mesh cell average of the true solution. Thus, if δ is the mesh cell width, then we should seek to approximate not the pointwise fluid velocity $\boldsymbol{u}(\mathbf{x}, t)$ but rather some mesh cell average $\overline{\boldsymbol{u}}(\mathbf{x}, t)$. The simplest such average is given by the convolution of

the velocity $\boldsymbol{u}$ with a rapidly decaying spatial filter $g_\delta(\mathbf{x})$. The most popular filters $g_\delta(\mathbf{x})$ are the sharp cut-off, box (top hat), Gaussian, and differential.

Then this is the idea of LES in a nutshell: pick a useful filter $g_\delta(\mathbf{x})$ and define $\overline{\boldsymbol{u}}(\mathbf{x},t) := (g_\delta * \boldsymbol{u})(\mathbf{x},t)$. Derive appropriate equations for $\overline{\boldsymbol{u}}$ by filtering the Navier-Stokes equations (NSE). Solve the closure problem. Impose accurate boundary conditions for $\overline{\boldsymbol{u}}$. Then discretize the resulting continuum model and solve it. Generally, such an averaging suppresses any fluctuations in $\boldsymbol{u}$ below $O(\delta)$ and preserves those on scales larger than $O(\delta)$.

In many flows, the portion of the flow that must be modeled, $\boldsymbol{u}' := \boldsymbol{u} - \overline{\boldsymbol{u}}$, is small relative to the portion that is calculated, $\overline{\boldsymbol{u}}$. Models in LES tend to be both simple and accurate, and the overall computational cost tends not to be much greater than doing an (unreliable, under-refined) solution of the NSE on the same mesh. This was the LES idea of deriving equations for space averaged variables mentioned by Richardson [27].

In the case of an incompressible fluid, the non-dimensionalized form of the Navier-Stokes equations (NSE) is

$$\boldsymbol{u}_t - Re^{-1}\Delta\boldsymbol{u} + (\boldsymbol{u}\cdot\nabla)\,\boldsymbol{u} + \nabla p = \boldsymbol{f}, \quad \text{in } \Omega, \tag{2.1}$$

$$\nabla\cdot\boldsymbol{u} = 0, \quad \text{in } \Omega, \tag{2.2}$$

$$\boldsymbol{u} = 0, \quad \text{on } \partial\Omega. \tag{2.3}$$

where $\boldsymbol{u}$ is the velocity, p is the pressure, and $Re := U\,L/\nu$ is the Reynolds number, defined as the ratio between the product of a characteristic length-scale L and a characteristic velocity U, and the kinematic viscosity ν.

To derive equations for $\overline{\boldsymbol{u}}$, we convolve the NSE with the chosen filter function $g_\delta(\mathbf{x})$. Using the fact that (for constant $\delta > 0$ and in the absence of boundaries) filtering commutes with differentiation, gives the space-filtered NSE:

$$\boldsymbol{u}_t - Re^{-1}\Delta\overline{\boldsymbol{u}} + \nabla\cdot(\overline{\boldsymbol{u}\,\boldsymbol{u}^T}) + \nabla\overline{p} = -\nabla\cdot\boldsymbol{\tau}(\boldsymbol{u},\boldsymbol{u}) \quad \text{in } \Omega\times(0,T), \tag{2.4}$$

$$\nabla\cdot\overline{\boldsymbol{u}} = 0 \quad \text{in } \Omega\times(0,T),. \tag{2.5}$$

This system is not closed, since it involves both $\boldsymbol{u}$ and $\overline{\boldsymbol{u}}$. The tensor $\boldsymbol{\tau}(\boldsymbol{u},\boldsymbol{u}) = \overline{\boldsymbol{u}\,\boldsymbol{u}^T} - \overline{\boldsymbol{u}}\,\overline{\boldsymbol{u}}^T$ or $\boldsymbol{\tau}_{ij}(\boldsymbol{u},\boldsymbol{u}) = \overline{\boldsymbol{u}_i\,\boldsymbol{u}_j} - \overline{\boldsymbol{u}}_i\,\overline{\boldsymbol{u}}_j$ is often called the subgrid-scale stress (SGS) tensor. Thus, the closure problem in LES is to model the SGS tensor $\boldsymbol{\tau}(\boldsymbol{u},\boldsymbol{u})$, i.e. to specify a tensor $\mathcal{S} = \mathcal{S}(\overline{\boldsymbol{u}},\overline{\boldsymbol{u}})$ to replace $\boldsymbol{\tau}(\boldsymbol{u},\boldsymbol{u})$ in (2.4).

2.1. Eddy Viscosity Models. The most popular approach to the closure problem is the Eddy Viscosity (EV) model. EV models are motivated by the idea that the global effect of the subfilter-scale stress tensor $\boldsymbol{\tau}(\boldsymbol{u},\boldsymbol{u})$, in the mean, is to transfer energy from resolved to unresolved scales through inertial interactions. EV models are motivated by Kolmogorov's (K-41) theory ([11, 24, 28]), and in particular by the *energy cascade*.

The essence of the energy cascade ([27]) is that kinetic energy enters the turbulent flow at the largest scales of motion, and is then transferred by inviscid processes to smaller and smaller scales, until it is eventually dissipated through viscous effects. Thus, the action of the subfilter-scale stress $\boldsymbol{\tau}$ is thought of as having a dissipative effect on the mean flow: the scales uncaptured on the numerical mesh (above the cut-off wavenumber k_c) should dissipate energy from the large scales (below the cut-off wavenumber k_c).

Boussinesq [5] first formulated the *EV/Boussinesq hypothesis* based upon an analogy between the interaction of small eddies and the perfectly elastic collision of

molecules (*e.g.*, molecular viscosity or heat): *"Turbulent fluctuations are dissipative in the mean."* The mathematical realization is the model

$$\nabla \cdot \boldsymbol{\tau}(\boldsymbol{u}, \boldsymbol{u}) \approx -\nabla \cdot (\nu_T \nabla^s \overline{\boldsymbol{u}}) + \text{ terms incorporated into } \overline{p},$$

where $\nabla^s \overline{\boldsymbol{u}} := (\nabla \overline{\boldsymbol{u}} + \nabla \overline{\boldsymbol{u}}^T)/2$ is the deformation tensor of $\overline{\boldsymbol{u}}$ and $\nu_T \geq 0$ is the "turbulent viscosity coefficient". The modeling problem then reduces to determining one parameter: the turbulent viscosity coefficient $\nu_T(\overline{\boldsymbol{u}}, \delta)$.

2.2. The Smagorinsky Model. The most common EV model is known in LES as the Smagorinsky model, in which

$$\nu_T = \nu_{\text{Smag}}(\overline{\boldsymbol{u}}, \delta) := (c_s \delta)^2 \|\nabla^s \overline{\boldsymbol{u}}\|_F, \tag{2.6}$$

where δ is the filter radius, c_s is the Smagorinsky constant, and $\|\sigma\|_F := \sqrt{\sum_{i,j=1}^{d} |\sigma_{ij}|^2}$ is the Frobenius norm of the tensor σ. This model was studied by [31] as a nonlinear artificial viscosity in gas dynamics and by [29] for geophysical flow calculations. A complete mathematical theory for partial differential equations involving this term was constructed by Ladyžhenskaya [18, 19].

Lilly [21] showed that, for isotropic, homogeneous turbulence, c_s has a simple, universal value 0.17 and is not a "tuning" constant. Defining the dissipation rate $\epsilon(t) = \frac{\nu}{|\Omega|}\|\nabla \boldsymbol{u}(t)\|^2$, Lilly's idea was to equate the dissipation rates $\langle \epsilon \rangle = \langle \epsilon_{\text{model}} \rangle$ and from this to determine a value for c_s. The Smagorinsky model (1.1) where $c_s \sim 0.17$ seems to be a universal answer in LES. It is easy to implement, stable, and (under "optimistic" assumptions) it replicates energy dissipation rates. Unfortunately, it can be also quite inaccurate for many problems.

The most successful form of the Smagorinsky model is the *dynamic* SGS model of [12], in which c_s is chosen locally in space and time, $c_s = c_s(\mathbf{x}, t)$. An essential improvement is that the dynamic SGS model introduces *backscatter* ([23]), the inverse transfer of energy from small scales to large scales. A yet improved version of the dynamic SGS model is the *Lagrangian dynamic* SGS model of [22, 25].

2.3. The Overly Diffusive Character of the Smagorinsky Model. Whether simplistic or more involved, all these approaches target the same defficiency of the Smagorinsky model - its overly diffusive character. This negative feature of the Smagorinsky model is clearly illustrated by the schematic in Figure 1. Plotting the amount of AV introduced by the Smagorinsky model against $\|\delta\, \mathbb{D}(\boldsymbol{u})\|$, we obtain a linear profile: Indeed, (1.1) can be rewritten as

$$\nu_T = \nu_{\text{Smag}}(\overline{\boldsymbol{u}}, \delta) = C_s^2\, \delta\, \|\delta\, \nabla^s \overline{\boldsymbol{u}}\|_F, \tag{2.7}$$

which yields a linear profile for ν_T (if δ is held constant). In smooth regions of the flow, where the deformation tensor is relatively small ($\|\mathbb{D}(\boldsymbol{u})\|_F \leq O(1/\delta)$), the Smagorinsky model will introduce a moderate amount of AV ($\nu_T \leq O(\delta)$). In those regions of the flow where the deformation tensor is large ($\|\mathbb{D}(\boldsymbol{u})\|_F \geq O(1/\delta^2)$, for example), the Smagorinsky model will introduce an *unphysical* amount of AV ($\nu_T \sim O(1)$).

The overly diffusive feature of the Smagorinsky model is manifest in practical computations of flows displaying a large deformation tensor, such as wall-bounded flows. Indeed, for turbulent channel flows and pipe flows, because the velocity deformation tensor is very large near the solid wall, the Smagorinsky model introduces an

unphysical amount of AV. (**References!!!!**) Similarly, in stratified flows with large shear (and thus, large deformation tensors), the Smagorinsky model introduces an unphysical amount of AV in the vertical direction. (**References!!!!**)

There have been numerous modifications of the Smagorinsky model, all trying to attenuate its overly diffusive character. The simplest such approach is the "clipping procedure"

$$\nu_T = \nu_{Smag}^{clipping}(\overline{\boldsymbol{u}}, \delta) := \max\{\nu_{Smag}(\overline{\boldsymbol{u}}, \delta), C\}, \tag{2.8}$$

where C is a user-defined constant. (**References!!!!**)

A more involved approach for wall-bounded flows (such as channel and pipe flows) is the Van Driest damping [30], in which

$$\nu_T = \nu_{Smag}^{VD}(\overline{\boldsymbol{u}}, \delta) := \left[\left(1 - e^{-\frac{y^+}{25}}\right)\right] \nu_{Smag}(\overline{\boldsymbol{u}}, \delta), \tag{2.9}$$

where y^+ is the nondimensionalized distance to the wall (see Chapter 12 in [4] for more details). The main improvement over the *ad hoc* clipping procedure 2.8 is that the damping function in 2.9 is chosen so that the resulting flow satisfy the turbulent boundary layer theory [24]. In stratified flows, the Smagorinsky model is used with a damping function in the vertical direction

$$\nu_T^z = \nu_{Smag}^{Ri}(\overline{\boldsymbol{u}}, \delta) := \sqrt{1 - \frac{Ri}{Ri_c}}\nu_{Smag}(\overline{\boldsymbol{u}}, \delta), \tag{2.10}$$

where Ri is the Richardson number given by the ratio of shear and buoyancy (**CHECK!!!!**), and Ri_c is a critical Richardson number (a popular choice is $Ri_c \sim 0.25$). (**References!!!!**)

2.4. The Bounded AV Model. We consider in this paper the bounded AV model, a general, mathematically sound alternative to the Smagorinsky model. The bounded AV model reads

$$\nu_T = \mu\delta^\sigma a(\delta|\nabla \boldsymbol{u}|)\nabla \boldsymbol{u}, \tag{2.11}$$

where $a(\cdot)$ is a general function whose graph ressembles that in Figure 1. This new model, proposed in [15] for convection-diffusion problems, is a clear improvement over the Smagorinsky model. Indeed, in the flow regions with large velocity deformation tensors, the bounded AV model introduces a *bounded* amount of AV, just enough to spread the solution onto the computational mesh. This is in clear contrast with the Smagorinsky model, which introduces an unbounded amount of AV, thus being overly dissipative. The improvement of the bounded AV model over the Smagorinsky model is clearly supported by the 2D and 3D channel flow experiments in Section 7.

The bounded AV model is very general. Indeed, the function $a(\cdot)$ in (1.2) is just required to be bounded and monotonically increasing (see Figure 1). Thus, the bounded AV model clearly includes as a particular case the *ad hoc* "clipped" Smagorinsky model (2.8). Although the bounded AV model does not directly include the Smagorinsky model with Van Driest damping (2.9) ($a(\cdot)$ must be monotonically increasing) or the Ri-dependent Smagorinsky model (2.10) ($a(\cdot)$ depends on $\nabla \boldsymbol{u}$, whereas (2.10) depends on $\frac{\partial \boldsymbol{u}}{\partial z}$), it is certainly related to these two models, targeting the overly diffusive character of the Smagorinsky model. Note also that, while models (2.9) and (2.10) are tailored for specific flows (wall-bounded and stratified, respectively), the bounded AV model is not restricted to any particular type of flow.

There are numerous challenges in the numerical analysis of LES, where the study of classic topics such as consistency, stability, and convergence of the LES discretization are still at an initial stage. Only the first few steps along these lines have been made, some of which are presented in the exquisite monograph of John [16].

A thorough numerical analysis for the finite element implementation of the Smagorinsky model has been presented in [9, 10]. Further studies have been presented in [20]. In [17], the authors have presented a rigorous numerical analysis for the popular claim that the Smagorinsky model yields error estimates which are independent of the Re.

In this paper, we present a rigorous numerical analysis for the finite element implementation of the bounded AV model for the NSE:

$$\boldsymbol{u}_t - Re^{-1}\Delta\boldsymbol{u} - \nabla\cdot(\mu\delta^\sigma a(\delta|\nabla\boldsymbol{u}|)\nabla\boldsymbol{u}) + (\boldsymbol{u}\cdot\nabla)\,\boldsymbol{u} - \nabla p = \boldsymbol{f}, \quad \text{in } \Omega, \tag{2.12}$$

$$\nabla\cdot\boldsymbol{u} = 0, \quad \text{in } \Omega, \tag{2.13}$$

$$\boldsymbol{u} = 0, \quad \text{on } \partial\Omega. \tag{2.14}$$

We also illustrate our error estimates through numerical simulations with the bounded AV model for 2D and 3D channel flows and the 2D vortex decay problem.

3. The Variational Formulation. In this section, we develop the variational formulation for (2.12)- (2.14). We will denote by $W^{m,p}(\Omega)$ the usual Sobolev spaces [**?**] with norms $\|\cdot\|_{W^{m,p}}$ and semi-norms $|\cdot|_{W^{m,p}}$, and set $H^m(\Omega) := W^{m,2}(\Omega)$ and $L^p(\Omega) := W^{0,p}(\Omega)$. In the sequel we will denote $\|\cdot\|$ and $(\cdot,\cdot)$ the norm and inner product for $L^2(\Omega)$, and $\|\cdot\|_m$ the norm for $H^m(\Omega)$.

Specifically, we use the following function spaces for the variational formulation:

$$\text{Velocity space} : \boldsymbol{X} := \boldsymbol{H}_0^1(\Omega) := \left\{\boldsymbol{v}\in\boldsymbol{H}^1(\Omega) \;:\; \boldsymbol{v} = 0 \; on \; \partial\Omega\right\},$$

$$\text{Pressure space} : Q := L_0^2(\Omega) := \left\{q\in L^2(\Omega) \;:\; \int_\Omega q dx = 0\right\}.$$

The variational formulation of (2.12)-(2.14) proceeds in the usual manner. Multiplying (2.12), (2.13) by a velocity ($\boldsymbol{v}$) and pressure (q) test function, respectively, integrating over Ω, and integrating by parts (using the fact that $\boldsymbol{v} = 0$ on $\partial\Omega$), we obtain

$$\begin{aligned}(\boldsymbol{u}_t,\boldsymbol{v}) + A(\boldsymbol{u},\boldsymbol{v}) + B(\boldsymbol{u},\boldsymbol{u},\boldsymbol{v})\\ +C(\boldsymbol{u},\boldsymbol{u},\boldsymbol{v}) - (p,\nabla\cdot\boldsymbol{v}) = (\boldsymbol{f},\boldsymbol{v}), \quad \forall\boldsymbol{v}\in\boldsymbol{X}, \quad t\in[0,T],\end{aligned} \tag{3.1}$$

$$(\nabla\cdot\boldsymbol{u},q) = 0, \qquad \forall q\in Q, \quad t\in[0,T] \tag{3.2}$$

where the bilinear form $A(\cdot,\cdot)$ is defined by

$$A(\boldsymbol{u},\boldsymbol{v}) := v\,(\nabla\boldsymbol{u},\nabla\boldsymbol{v}),$$

and the trilinear forms $B(\cdot,\cdot,\cdot)$ and $C(\cdot,\cdot,\cdot)$ are defined by

$$B(\boldsymbol{u},\boldsymbol{v},\boldsymbol{w}) := \mu\delta^\sigma\,(a(\delta|\nabla\boldsymbol{u}|)\nabla\boldsymbol{v},\nabla\boldsymbol{w}),$$

$$C(\boldsymbol{u},\boldsymbol{v},\boldsymbol{w}) := (\boldsymbol{u}\cdot\nabla\boldsymbol{v},\boldsymbol{w}).$$

In addition, note that the velocity and pressure spaces, $\boldsymbol{X}$ and Q, satisfy the *inf-sup* condition

$$\inf_{q\in Q}\sup_{\boldsymbol{v}\in\boldsymbol{X}}\frac{(q,\nabla\cdot\boldsymbol{v})}{\|q\|\|v\|_1} \geq \beta > 0.$$

3.1. Finite Element Spaces. Let $\Omega \subset \mathbb{R}^{\mathrm{d}}$, $(\mathrm{d} = 2, 3)$ be a polygonal domain and let T_h denote a triangulation of Ω made up of triangles (in $\mathbb{R}^2$) or tetrahedrals (in $\mathbb{R}^3$). Thus, the computational domain is defined by

$$\Omega = \bigcup K, \quad K \in T_h.$$

We also assume that for a particular triangulation T_h of Ω, there exist constants c_1, c_2 such that

$$c_1 h \leq h_K \leq c_2 \rho_K,$$

where h_K is the diameter of K, ρ_K is the diameter of the greatest ball (sphere) included in K and $h = \max_{K \in T_h} h_K$. Let $P_K(A)$ denote the space of polynomials on A of degree no greater than k. Then we define the finite element spaces associated with the velocity and pressure spaces as follows.

$$\begin{aligned} \boldsymbol{X}_h &:= \left\{ \boldsymbol{v} \in \boldsymbol{X} \cap C(\bar{\Omega})^d : \boldsymbol{v}\big|_K \in P_k(K),\ \forall K \in T_h \right\}, \\ Q_h &:= \left\{ q \in Q \cap C(\bar{\Omega}) : q\big|_K \in P_q(K),\ \forall K \in T_h \right\}, \end{aligned}$$

where $C(\bar{\Omega})$ denotes the set of continuous functions on the closure of Ω. Analogous to the continuous *inf-sup* condition, we also assume that the spaces $\boldsymbol{X}_h, Q_h$ satisfy the *discrete inf-sup* condition

$$\inf_{q \in Q_h} \sup_{\boldsymbol{v} \in \boldsymbol{X}_h} \frac{(q, \nabla \cdot \boldsymbol{v})}{\|q\| \|v\|_1} \geq \beta > 0.$$

We now note the usual approximation properties for the finite element spaces $\boldsymbol{X}_h, Q_h$. For $(\boldsymbol{u}, p) \in \boldsymbol{H}^{k+1}(\Omega) \times H^{q+1}(\Omega)$, we have that the interpolants $(I_h \boldsymbol{u}, I_h p) \in \boldsymbol{X}_h \times Q_h$ satisfy

$$\begin{aligned} \|\boldsymbol{u} - I_h \boldsymbol{u}\| &\leq C_I h^{k+1} |\boldsymbol{u}|_{\boldsymbol{H}^{k+1}}, \\ \|\boldsymbol{u} - I_h \boldsymbol{u}\|_1 &\leq C_I h^{k} |\boldsymbol{u}|_{\boldsymbol{H}^{k+1}}, \\ \|p - I_h p\| &\leq C_I h^{q} |p|_{H^{q+1}}. \end{aligned}$$

From [**?**], we have the following results

LEMMA 3.1. *Let $\{T_h\}$ $0 < h \leq 1$ denote a quasi-uniform family of subdivisions of a polyhedral domain $\Omega \subset \mathbb{R}^{\mathrm{d}}$. Let $(\hat{K}, P, N)$ be a reference finite element such that $P \subset W^{l,p}(\hat{K}) \cap W^{m,q}(\hat{K})$ where $1 \leq p, q \leq \infty$ and $0 \leq m \leq l$. For $K \in T_h$, let (K, P_K, N_K) be the affine equivalent element, and $V_h = \left\{ v \ : \ v \text{ is measurable and } v\Big|_K \in P_K,\ \forall K \in T_h \right\}$. Then there exists $C = C(l, p, q)$ such that*

$$\left[\sum_{K \in T_h} \|v\|^p_{W^{l,p}(K)} \right]^{1/p} \leq C h^{m-l+min\left(0, \frac{d}{p} - \frac{d}{q}\right)} \left[\sum_{K \in T_h} \|v\|^q_{W^{m,q}(K)} \right]^{1/q}. \tag{3.3}$$

LEMMA 3.2. *Let $I_h v$ denote the interpolant of v. Then for all $v \in W^{m,p}(\Omega) \cap C^r(\Omega)$ and $0 \leq s \leq \min\{m, r+1\}$,*

$$\|v - I_h v\|_{W^{s,\infty}} \leq C h^{m-s-d/p} |v|_{W^{m,p}}.$$

4. Stability Results. In this section, we prove some stability results concerning the variational problem (3.1)-(3.2), as well as its semi-discrete finite element approximation. Useful in the following analysis are the following three lemmas.

LEMMA 4.1. *[15] For $\boldsymbol{u}, \boldsymbol{v} \in \boldsymbol{X}$, and the function $a(\cdot)$ satisfying*

$$0 \le a(x) \le 1, \qquad a'(x) \ge 0, \qquad \forall\ x \in [0, \infty),$$

we have

$$B(\boldsymbol{u}, \boldsymbol{u}, \boldsymbol{u} - \boldsymbol{v}) - B(\boldsymbol{v}, \boldsymbol{v}, \boldsymbol{u} - \boldsymbol{v}) \ge 0$$

Proof. Consider the functional $I : \boldsymbol{X} \to \mathbb{R}$, defined by

$$I(\boldsymbol{U}) := \int_\Omega A(|\nabla \boldsymbol{U}|) dx,$$

where the function $A : [0, \infty) \to \mathbb{R}$ is defined by

$$A(x) := \int_0^x t\, a(t) dt.$$

First, note that

$$dI(\boldsymbol{U}, \boldsymbol{V}) = \int_\Omega A'(|\boldsymbol{U}|) \frac{\nabla \boldsymbol{U}}{|\nabla \boldsymbol{U}|} \nabla \boldsymbol{V}\, dx = \int_\Omega a(|\nabla \boldsymbol{U}|) \nabla \boldsymbol{U} \nabla \boldsymbol{V}\, dx,$$

where $dI(\boldsymbol{U}, \boldsymbol{V})$ is the Gâteaux derivative of I at $\boldsymbol{U}$ in the direction of $\boldsymbol{V}$.

Therefore, setting $\boldsymbol{U}_1 := \delta \boldsymbol{u}$, $\boldsymbol{U}_2 := \delta \boldsymbol{v}$, and $\boldsymbol{V} := \boldsymbol{U}_1 - \boldsymbol{U}_2$, we have

$$B(\boldsymbol{u}, \boldsymbol{u}, \boldsymbol{u} - \boldsymbol{v}) - B(\boldsymbol{v}, \boldsymbol{v}, \boldsymbol{u} - \boldsymbol{v}) = \frac{\mu \delta^\sigma}{\delta^2} \left(dI(\boldsymbol{U}_1, \boldsymbol{V}) - dI(\boldsymbol{U}_2, \boldsymbol{V}) \right). \tag{4.1}$$

However, we can rewrite this expression as

$$\begin{aligned}
&dI(\boldsymbol{U}_1, \boldsymbol{V}) - dI(\boldsymbol{U}_2, \boldsymbol{V}) = \int_0^1 \frac{d}{dt} dI(\boldsymbol{U}_2 + t(\boldsymbol{U}_1 - \boldsymbol{U}_2), \boldsymbol{V})\, dt \\
&= \int_0^1 \frac{d}{dt} \int_\Omega a(|\nabla(\boldsymbol{U}_2 + t(\boldsymbol{U}_1 - \boldsymbol{U}_2|)) \nabla(\boldsymbol{U}_2 + t(\boldsymbol{U}_1 - \boldsymbol{U}_2)) \nabla \boldsymbol{V}\, dx\, dt \\
&= \int_0^1 \int_\Omega a'(|\nabla(\boldsymbol{U}_2 + t(\boldsymbol{U}_1 - \boldsymbol{U}_2|) \frac{\nabla(\boldsymbol{U}_2 + t(\boldsymbol{U}_1 - \boldsymbol{U}_2) \nabla \boldsymbol{V}) \nabla \boldsymbol{V}}{|\nabla(\boldsymbol{U}_2 + t(\boldsymbol{U}_1 - \boldsymbol{U}_2)) \nabla \boldsymbol{V}|} \nabla(\boldsymbol{U}_2 + t(\boldsymbol{U}_1 - \boldsymbol{U}_2) \nabla \boldsymbol{V}\, dx\, dt \\
&\quad + \int_0^1 \int_\Omega a(|\nabla(\boldsymbol{U}_2 + t(\boldsymbol{U}_1 - \boldsymbol{U}_2))|) |\nabla \boldsymbol{V}|^2\, dx\, dt.
\end{aligned} \tag{4.2}$$

As $a(x), a'(x) \ge 0$, it is clear that the expression in (4.2) is nonnegative. Finally, using (4.1) we obtain the stated result. ∎

LEMMA 4.2. *For $\boldsymbol{u}_1, \boldsymbol{u}_2, \boldsymbol{v}, \boldsymbol{w} \in \boldsymbol{X}$, and the function $a(\cdot)$ satisfying*

$$0 \le a(x) \le 1, \qquad 0 \le a'(x) \le M_a, \qquad \forall\ x \in [0, \infty),$$

we have

$$|B(\boldsymbol{u}_1, \boldsymbol{v}, \boldsymbol{w}) - B(\boldsymbol{u}_2, \boldsymbol{v}, \boldsymbol{w})| \le M_a \mu \delta^{\sigma+1} |(|\nabla \boldsymbol{u}_1 - \nabla \boldsymbol{u}_2| \nabla \boldsymbol{v}, \nabla \boldsymbol{w})| \tag{4.3}$$

and

$$|B(\boldsymbol{u}_1, \boldsymbol{v}, \boldsymbol{w})| \leq M_a \mu \delta^{\sigma+1} \left|(|\nabla \boldsymbol{u}_1| \nabla \boldsymbol{v}, \nabla \boldsymbol{w})\right| \tag{4.4}$$

Proof. Without loss of generality, we assume that $|\nabla \boldsymbol{u}_1| \geq |\nabla \boldsymbol{u}_2|$. Immediately, we have

$$|B(\boldsymbol{u}_1, \boldsymbol{v}, \boldsymbol{w}) - B(\boldsymbol{u}_2, \boldsymbol{v}, \boldsymbol{w})| = \mu \delta^{\sigma} \left|(|a(\delta|\nabla \boldsymbol{u}_1|) - a(\delta|\nabla \boldsymbol{u}_2|)| \nabla \boldsymbol{v}, \nabla \boldsymbol{w})\right|. \tag{4.5}$$

Now, by the mean value theorem, we have that there exists $c_a \in [|\nabla \boldsymbol{u}_2|, |\nabla \boldsymbol{u}_1|]$, such that

$$|a(\delta|\nabla \boldsymbol{u}_1|) - a(\delta|\nabla \boldsymbol{u}_2|)| = a'(c_a)(|\nabla \boldsymbol{u}_1| - |\nabla \boldsymbol{u}_2|).$$

Combining this with the reverse triangle inequality, $||x| - |y|| \leq |x - y|$, we have

$$|a(\delta|\nabla \boldsymbol{u}_1|) - a(\delta|\nabla \boldsymbol{u}_2|)| \leq a'(c_a)|\nabla \boldsymbol{u}_1 - \nabla \boldsymbol{u}_2|. \tag{4.6}$$

Finally, substituting (4.6) into (4.5) and noting that $a'(c_a) \leq M_a$, we obtain (4.3). The result (4.4) follows directly. ∎

LEMMA 4.3. *(Leray's inequality) A solution of (3.1)-(3.2) satisfies*

$$\frac{1}{2}\|\boldsymbol{u}(t)\|^2 + \int_0^t v\|\nabla \boldsymbol{u}\|^2 dt' \leq \frac{1}{2}\|\boldsymbol{u}(0)\|^2 + \int_0^t (\boldsymbol{f}, \boldsymbol{u}) dt'.$$

Proof. The stated result follows by setting $\boldsymbol{v} = \boldsymbol{v}$ and $q = p$ in (3.1) and (3.2), noting that

$$B(\boldsymbol{u}, \boldsymbol{u}, \boldsymbol{u}) \geq 0, \qquad C(\boldsymbol{u}, \boldsymbol{u}, \boldsymbol{u}) = 0,$$

and integrating from 0 to t. ∎

We now establish the semi-discrete approximation as the solution of (3.1)- (3.2) restricted to the finite element spaces $\boldsymbol{X}_h, Q_h$.

Definition [Semi-Discrete Approximation] The semi-discrete approximation is defined to be an element $(\boldsymbol{u}_h, p_h) \in C(0,T;\boldsymbol{X}_h) \cap C(0,T;Q_h)$ such that

$$\begin{aligned}(\boldsymbol{u}_{h,t}, \boldsymbol{v}) + A(\boldsymbol{u}_h, \boldsymbol{v}) + B(\boldsymbol{u}_h, \boldsymbol{u}_h, \boldsymbol{v}) \\ +C(\boldsymbol{u}_h, \boldsymbol{u}_h, \boldsymbol{v}) - (p_h, \nabla \cdot \boldsymbol{v}) = (\boldsymbol{f}, \boldsymbol{v}), \quad \forall \boldsymbol{v} \in \boldsymbol{X}_h, \quad t \in [0,T], \qquad (4.7)\\ (\nabla \cdot \boldsymbol{u}_h, q) = 0, \qquad \forall q \in Q_h, \quad t \in [0,T]. \qquad (4.8)\end{aligned}$$

We immediately obtain the following two lemmas.

LEMMA 4.4. *(Leray's inequatity for $\boldsymbol{u}_h$.) A solution of (4.7)-(4.8) satisfies*

$$\frac{1}{2}\|\boldsymbol{u}_h(t)\|^2 + \int_0^t v\|\nabla \boldsymbol{u}_h\|^2 dt' \leq \frac{1}{2}\|\boldsymbol{u}_h(0)\|^2 + \int_0^t (\boldsymbol{f}, \boldsymbol{u}_h) dt'.$$

Proof. Setting $\boldsymbol{v} = \boldsymbol{u}_h$ and $q = p_h$ in (4.7)-(4.8), we immediately have

$$\frac{1}{2}\frac{d}{dt}\|\boldsymbol{u}_h(t)\|^2 + v\|\nabla \boldsymbol{u}_h\|^2 \leq (\boldsymbol{f}, \boldsymbol{u}_h). \tag{4.9}$$

Integrating from 0 to t thus yields the stated result. ∎

LEMMA 4.5. *(Stability of $\boldsymbol{u}_h$.) A solution of (4.7)-(4.8) satisfies*

$$\|\boldsymbol{u}_h\|_{L^\infty(0,T,L^2(\Omega))} \leq C(\|f\|_{L^2(0,T;H^{-1}(\Omega))} + \|\boldsymbol{u}(0)\|_{L^2(\Omega)}. \tag{4.10}$$

Furthermore, there exists $\alpha > 0$ such that

$$\|\boldsymbol{u}_h(t)\|_{L^2(\Omega)} \leq e^{-\alpha t}\|\boldsymbol{u}_h(0)\|_{L^2(\Omega)} + \int_0^t e^{-\alpha(t-s)}\|\boldsymbol{f}(s)\|_{H^{-1}(\Omega)}, \quad \forall\ t > 0. \tag{4.11}$$

Also, we have that $\boldsymbol{u}_h(t) \in L^\infty(\Omega)$ for all $t > 0$.

Proof. Using (4.9) and the fact that

$$(\boldsymbol{f}, \boldsymbol{u}_h) \leq \frac{1}{4\epsilon}\|\boldsymbol{f}\|^2_{H^{-1}(\Omega)} + \epsilon\|\boldsymbol{u}\|^2_{H^1(\Omega)},$$

we have

$$\frac{d}{dt}\|\boldsymbol{u}_h\|^2 + C_1\|\boldsymbol{u}_m\|^2_{H^1(\Omega)} \leq C_2\|\boldsymbol{f}\|^2_{H^{-1}(\Omega)}. \tag{4.12}$$

Therefore, the estimate (4.10) directly follows from dropping the $\|\boldsymbol{u}_m\|^2_{H^1(\Omega)}$ from (4.12) and integrating from 0 to t.

Next, to obtain the estimate (4.11), we note that by Poincaré's inequality, $\|\boldsymbol{u}\|_{L^2} \leq C\|\nabla\boldsymbol{u}\|_{L^2}$,

$$\frac{d}{dt}\|\boldsymbol{u}_h\|^2 + C_0\|\boldsymbol{u}_m\|^2_{L^2(\Omega)} \leq C_2\|\boldsymbol{f}\|^2_{H^{-1}(\Omega)}. \tag{4.13}$$

Therefore, inequality (4.11) follows by using an integrating factor.

Finally, from (4.12) we have that

$$\|\nabla\boldsymbol{u}_h\| \leq C\|\boldsymbol{f}\|_{H^{-1}(\Omega)}.$$

The interpolation property (3.3) implies therefore, that

$$\|\boldsymbol{u}_h\|_{L^\infty(\Omega)} \leq Ch^{1-d/2}\|\boldsymbol{f}\|_{H^{-1}(\Omega)}.$$

∎

5. An *A Priori* Error Estimate. In order to prove an *a priori* error estimate for the semi-discrete approximation $(\boldsymbol{u}_h, p_h)$, we must assume that the solution to the continuous problem satisfies $\|\boldsymbol{u}\|_{L^\infty}, \|\nabla\boldsymbol{u}\|_{L^\infty} \leq M$.

THEOREM 5.1. *Assume that the system (3.1)-(3.2) has a solution $(\boldsymbol{u}, p) \in \boldsymbol{X} \times Q$ which satifies*

$$\|\boldsymbol{u}\|_{L^\infty}, \|\nabla\boldsymbol{u}\|_{L^\infty} \leq M, \ \forall\ t \in [0,T].$$

Then, the semidiscrete approximation (4.7)-(4.8) is convergent to the solution of (3.1)-(3.2) on the interval $(0,T)$ as $h \to 0$. In addition, the approximation $(\boldsymbol{u}_h, p_h)$ satisfies the following error estimate

$$\|\boldsymbol{u} - \boldsymbol{u}_h\|^2_{L^\infty(0,T;L^2(\Omega))} + \|\nabla(\boldsymbol{u} - \boldsymbol{u}_h)\|^2_{L^2(0,T;L^2(\Omega))}$$
$$\leq C\left(\|\boldsymbol{u}(0) - \boldsymbol{u}_h(0)\|^2 + \inf_{\boldsymbol{v}\in\boldsymbol{X}_h, q\in Q}\mathcal{F}(\boldsymbol{u}-\boldsymbol{v}, p-q)\right), \tag{5.1}$$

where

$$\mathcal{F}(\boldsymbol{u}-\boldsymbol{v},p-q) := \|\boldsymbol{u}-\boldsymbol{v}\|_{L^\infty(0,T;L^2(\Omega))} + \|(\boldsymbol{u}-\boldsymbol{v})_t\|^2_{L^\infty(0,T;L^2(\Omega))} + \|\nabla(\boldsymbol{u}-\boldsymbol{v})\|_{L^2(0,T,L^2(\Omega))} + \|p-q\|_{L^\infty(0,T;L^2(\Omega))}.$$

Proof. We begin by defining the following quantities

$$\epsilon_u := \boldsymbol{u}-\boldsymbol{u}_h, \quad \phi := \boldsymbol{U}-\boldsymbol{u}_h, \quad \eta := \boldsymbol{u}-\boldsymbol{U},$$

where $\boldsymbol{U}$ is some member of $\boldsymbol{X}_h$ such that $\|\boldsymbol{U}\|_{L^\infty}, \|\nabla \boldsymbol{U}\|_{L^\infty} \leq \tilde{M}$. Note that this must be true of the interpolant satisfying the RHS of (5.1).

First, subtracting (4.7) from (3.1), we have

$$(\epsilon_u,\boldsymbol{v})+A(\epsilon_u,\boldsymbol{v})+B(\boldsymbol{u},\boldsymbol{u},\boldsymbol{v})-B(\boldsymbol{u}_h,\boldsymbol{u}_h,\boldsymbol{v})+C(\boldsymbol{u},\boldsymbol{u},\boldsymbol{v})-C(\boldsymbol{u}_h,\boldsymbol{u}_h,\boldsymbol{v})-(p-p_h,\nabla\cdot\boldsymbol{v}) = 0.$$

Next, noting that $\epsilon_u = \phi+\eta$ and setting $\boldsymbol{v}=\phi$, we have

$$(\phi_t,\phi) + A(\phi_t,\phi) + B(\boldsymbol{U},\boldsymbol{U},\phi) - B(\boldsymbol{u}_h,\boldsymbol{u}_h,\phi) = \boldsymbol{G}(\phi), \tag{5.2}$$

where

$$\begin{aligned}\boldsymbol{G}(\phi) := &-(\eta_t,\phi) - A(\eta,\phi)\\ &-(B(\boldsymbol{u},\boldsymbol{u},\phi) - B(\boldsymbol{U},\boldsymbol{U},\phi))\\ &-(C(\boldsymbol{u},\boldsymbol{u},\phi) - C(\boldsymbol{U},\boldsymbol{U},\phi))\\ &-(C(\boldsymbol{U},\boldsymbol{U},\phi) - C(\boldsymbol{u}_h,\boldsymbol{u}_h,\phi))\\ &+(p-p_h,\nabla\cdot\phi)\\ = &\text{ (I) + (II) + (III) + (IV) + (V) + (VI).}\end{aligned}$$

First we note that (5.2) may be rewritten as

$$\frac{1}{2}\frac{d}{dt}\|\phi\|^2 + v\|\nabla\phi\|^2 \leq \boldsymbol{G}(\phi),$$

as $B(\boldsymbol{U},\boldsymbol{U},\phi) - B(\boldsymbol{u}_h,\boldsymbol{u}_h,\phi) \geq 0$ by Lemma 4.1.

What remains is to estimate each of the terms in $\boldsymbol{G}(\phi)$.

$$\text{(I)} \leq |(\eta_t,\phi)| \leq \frac{1}{2}\|\phi\|^2 + \frac{1}{2}\|\eta_t\|^2.$$

$$\begin{aligned}\text{(II)} \leq |A(\eta,\phi)| &\leq v\|\nabla\eta\|\|\nabla\phi\|\\ &\leq \epsilon_1\|\nabla\phi\|^2 + \frac{1}{4\epsilon_1}\|\nabla\eta\|^2.\end{aligned}$$

$$\begin{aligned}\text{(III)} &\leq |B(\boldsymbol{u},\boldsymbol{u},\phi) - B(\boldsymbol{U},\boldsymbol{u},\phi)| + |B(\boldsymbol{U},\boldsymbol{u},\phi) - B(\boldsymbol{U},\boldsymbol{U},\phi)|\\ &= |B(\boldsymbol{u},\boldsymbol{u},\phi) - B(\boldsymbol{U},\boldsymbol{u},\phi)| + |B(\boldsymbol{U},\eta,\phi)|.\end{aligned}$$

Using Lemma 4 in each of these terms gives

$$\begin{aligned}|B(\boldsymbol{u},\boldsymbol{u},\phi) - B(\boldsymbol{U},\boldsymbol{u},\phi)| &\leq M_a\mu\delta^{\sigma+1}(|\nabla\eta|\nabla\boldsymbol{u},\nabla\boldsymbol{\phi})\\ &\leq M_a\mu\delta^{\sigma+1}\|\nabla\phi\|\,\||\nabla\eta|\nabla\boldsymbol{u}\|\\ &\leq M_a\mu\delta^{\sigma+1}\|\nabla\phi\|\,M\|\nabla\eta\|\\ &\leq \epsilon_2\|\nabla\phi\|^2 + \frac{C}{\epsilon_2}\|\nabla\eta\|^2,\end{aligned}$$

and

$$\begin{aligned}|B(\boldsymbol{U},\eta,\phi)| &\le M_a\mu\delta^{\sigma+1}(|\nabla\boldsymbol{U}|\nabla\eta,\nabla\boldsymbol{\phi})\\ &\le M_a\mu\delta^{\sigma+1}\|\nabla\phi\|\,\||\nabla\boldsymbol{U}|\nabla\eta\|\\ &\le M_a\mu\delta^{\sigma+1}\|\nabla\phi\|\,\tilde{M}\|\nabla\eta\|\\ &\le \epsilon_3\|\nabla\phi\|^2+\frac{C}{\epsilon_3}\|\nabla\eta\|^2.\end{aligned}$$

$$\begin{aligned}\text{(IV)} &\le |C(\boldsymbol{u},\boldsymbol{u},\phi)-C(\boldsymbol{U},\boldsymbol{u},\phi)|+|C(\boldsymbol{U},\boldsymbol{u},\phi)-C(\boldsymbol{U},\boldsymbol{u},\phi)|\\ &= |C(\eta,\boldsymbol{u},\phi)|+|C(\boldsymbol{U},\eta,\phi)|\end{aligned}$$

Estimating each of these terms, we get

$$\begin{aligned}|C(\eta,\boldsymbol{u},\phi)| &= |(\eta\cdot\nabla\boldsymbol{u},\phi)|\\ &\le \|\phi\|\,\|\eta\cdot\nabla\boldsymbol{u}\|\\ &\le \|\phi\|\,d^{1/2}M\|\eta\|\\ &\le \frac{M^2d}{2}\|\phi\|^2+\frac{M^2d}{2}\|\eta\|^2.\end{aligned}$$

$$\begin{aligned}|C(\boldsymbol{U},\eta,\phi)| &= |(\boldsymbol{U}\cdot\nabla\eta,\phi)|\\ &\le \|\phi\|\,\|\boldsymbol{U}\cdot\nabla\eta\|\\ &\le \|\phi\|\,d^{1/2}\tilde{M}\|\nabla\eta\|\\ &\le \frac{\tilde{M}^2d}{2}\|\phi\|^2+\frac{\tilde{M}^2d}{2}\|\nabla\eta\|^2.\end{aligned}$$

$$\begin{aligned}\text{(V)} &\le |C(\boldsymbol{U},\boldsymbol{U},\phi)-C(\boldsymbol{u}_h,\boldsymbol{U},\phi)|+|C(\boldsymbol{u}_h,\boldsymbol{U},\phi)-C(\boldsymbol{u}_h,\boldsymbol{u}_h,\phi)|\\ &= |C(\phi,\boldsymbol{U},\phi)|+|C(\boldsymbol{u}_h,\phi,\phi)|.\end{aligned}$$

Estimating each of these terms (and using the fact that $\|\boldsymbol{u}_h\|_{L^\infty}\le C_u$), we have

$$|C(\phi,\boldsymbol{U},\phi)| = |(\phi\cdot\nabla\boldsymbol{U},\phi)| \le dM^2\|\phi\|^2,$$

$$\begin{aligned}|C(\boldsymbol{u}_h,\phi,\phi)| &= |(\boldsymbol{u}_h\cdot\nabla\phi,\phi)|\\ &\le \|\phi\|\,\|\boldsymbol{u}_h\cdot\nabla\phi\|\\ &\le \|\phi\|\,C_u d^{1/2}\|\nabla\phi\|\\ &\le \epsilon_4\|\nabla\phi\|^2+\frac{C}{\epsilon_4}\|\phi\|^2.\end{aligned}$$

$$\begin{aligned}\text{(VI)} &= (p-p_h,\nabla\cdot\phi)\\ &= (p,\nabla\cdot\phi)\\ &= (p-P,\nabla\cdot\phi),\end{aligned}$$

where P is some element of Q_h, (using the mass equation). Therefore,

$$\begin{aligned}\text{(VI)} &\le \|p-P\|\|\nabla\cdot\phi\|\\ &\le \|p-P\|\,d^{1/2}\|\nabla\phi\|\\ &\le \epsilon_5\|\nabla\phi\|^2+\frac{C}{\epsilon_5}\|p-P\|^2.\end{aligned}$$

Now, we can combine all of the estimates for (I) - (VI) (appropriately choosing $\epsilon_1 - \epsilon_5$) to obtain

$$\frac{1}{2}\frac{d}{dt}\|\phi\|^2 + C_1\|\nabla\phi\|^2 \leq C_2\|\phi\|^2 + C_3\|\eta_t\|^2 + C_4\|\eta\|^2 + C_5\|\nabla\eta\|^2 + C_6\|p-P\|^2.$$

Applying Gronwall's lemma, we have for almost all $t \in [0,T]$,

$$\|\phi(t)\|^2 + C_1\|\nabla\phi\|^2_{L^2(0,t;L^2(\Omega))} \leq C_7\left(\|\phi(0)\|^2 + \|\eta_t\|^2 + \|\eta\|^2 + \|\nabla\eta\|^2 + \|p-P\|^2\right).$$

Thus, estimate (5.1) follows by setting $(\boldsymbol{U}, P)$ to be the element of $(\boldsymbol{X}_h, Q_h)$ in the RHS of (5.1), and noting that

$$\|\boldsymbol{u} - \boldsymbol{u}_h\|_{L^\infty(0,T;L^2(\Omega))} \leq \|\phi\|_{L^\infty(0,T;L^2(\Omega))} + \|\eta\|_{L^\infty(0,T;L^2(\Omega))}$$

and

$$\|\nabla(\boldsymbol{u} - \boldsymbol{u}_h)\|_{L^2(0,T;L^2(\Omega))} \leq \|\nabla\phi\|_{L^2(0,T;L^2(\Omega))} + \|\nabla\eta\|_{L^2(0,T;L^2(\Omega))}.$$

■

6. Newton Approximation Scheme for the Bounded AV Model. In this section, we discuss the Newton approximation scheme as applied to the Navier-Stokes equations with bounded artificial viscosity term. Note that approximate solutions $\boldsymbol{u}_h, p_h \in \boldsymbol{X}_h \times Q_h$ must satisfy a nonlinear system. In this section, we derive the Newton approximation scheme for the semi-discrete variational problem, and note that, in practice, one would apply a Newton iteration at each time step for a fully discrete approximation.

We first derive the Gateaux derivative for the bounded artificial viscosity term considered in this paper.

THEOREM 6.1. *Suppose that the function $a(\cdot) : \mathcal{R} \to \mathcal{R}$ is analytic, and define the (continuous) map $\mathcal{G}_1 : \boldsymbol{X}_h \to \boldsymbol{X}_h$ as*

$$\langle \mathcal{G}_1[\boldsymbol{u}], \boldsymbol{v}\rangle := (a(|\nabla\boldsymbol{u}|)\nabla\boldsymbol{u}, \nabla\boldsymbol{v}).$$

Then the Gâteaux derivative in the direction of $\boldsymbol{u}$ evaluated at $\boldsymbol{w}$, denoted as $\mathcal{J}_{\boldsymbol{u}}\mathcal{G}_1[\boldsymbol{w}]$ is equal to

$$\langle \mathcal{J}_{\boldsymbol{u}}\mathcal{G}_1[\boldsymbol{w}], \boldsymbol{v}\rangle = (a(|\nabla\boldsymbol{u}|)\nabla\boldsymbol{w}, \nabla\boldsymbol{v}) + \left(\frac{a'(|\nabla\boldsymbol{u}|)}{|\nabla\boldsymbol{u}|}[\nabla\boldsymbol{u} : \nabla\boldsymbol{w}]\nabla\boldsymbol{u}, \nabla\boldsymbol{v}\right)$$

Proof. Under the assumption that $a(\cdot)$ is analytic, we have a Taylor series expansion

$$a(x) = \sum_{n=0}^{\infty} \frac{a^{(n)}(0)\, x^n}{n!}.$$

Therefore,

$$\langle \mathcal{G}_1[\boldsymbol{u}], \boldsymbol{v}\rangle = \sum_{n=0}^{\infty} \frac{a^{(n)}(0)}{n!}\left(|\nabla\boldsymbol{u}|^n\nabla\boldsymbol{u}, \nabla\boldsymbol{v}\right).$$

For $n = 0$, it is clear that

$$\langle \mathcal{J}_{\boldsymbol{u}}\nabla\boldsymbol{w}, \nabla\boldsymbol{v}\rangle = (\nabla\boldsymbol{w}, \nabla\boldsymbol{v}),$$

and we have the formula for generic $n \geq 1$,

$$\langle \mathcal{J}_{\boldsymbol{u}} |\nabla \boldsymbol{w}|^n \nabla \boldsymbol{w}, \nabla \boldsymbol{v} \rangle = (|\nabla \boldsymbol{u}|^n \nabla \boldsymbol{w}, \nabla \boldsymbol{v}) + n \left(|\nabla \boldsymbol{u}|^{n-2} [\nabla \boldsymbol{u} : \nabla \boldsymbol{w}] \nabla \boldsymbol{u}, \nabla \boldsymbol{v} \right).$$

Therefore, we have that

$$\begin{aligned}
\langle \mathcal{J}_{\boldsymbol{u}} \mathcal{G}_1[\boldsymbol{w}], \boldsymbol{v} \rangle &= \sum_{n=0}^{\infty} \frac{a^{(n)}(0)}{n!} (|\nabla \boldsymbol{u}|^n \nabla \boldsymbol{w}, \nabla \boldsymbol{v}) + \sum_{n=1}^{\infty} \frac{n\, a^{(n)}(0)}{n!} \left(|\nabla \boldsymbol{u}|^{n-2} [\nabla \boldsymbol{u} : \nabla \boldsymbol{w}] \nabla \boldsymbol{u}, \nabla \boldsymbol{v} \right) \\
&= \sum_{n=0}^{\infty} \frac{a^{(n)}(0)}{n!} (|\nabla \boldsymbol{u}|^n \nabla \boldsymbol{w}, \nabla \boldsymbol{v}) + \sum_{n=1}^{\infty} \frac{a^{(n)}(0)}{(n-1)!} \left(\frac{|\nabla \boldsymbol{u}|^{n-1}}{|\nabla \boldsymbol{u}|} [\nabla \boldsymbol{u} : \nabla \boldsymbol{w}] \nabla \boldsymbol{u}, \nabla \boldsymbol{v} \right) \\
&= (a(|\nabla \boldsymbol{u}|) \nabla \boldsymbol{w}, \nabla \boldsymbol{v}) + \left(\frac{a'(|\nabla \boldsymbol{u}|)}{|\nabla \boldsymbol{u}|} [\nabla \boldsymbol{u} : \nabla \boldsymbol{w}] \nabla \boldsymbol{u}, \nabla \boldsymbol{v} \right)
\end{aligned}$$

■

COROLLARY 6.2. *Suppose that the function $a(\cdot) : \mathcal{R} \to \mathcal{R}$ is analytic, and define the (continuous) map $\mathcal{G}_2 : \boldsymbol{X}_h \to \boldsymbol{X}_h$ as*

$$\langle \mathcal{G}_2[\boldsymbol{u}], \boldsymbol{v} \rangle := (a(\delta |\nabla \boldsymbol{u}|) \nabla \boldsymbol{u}, \nabla \boldsymbol{v}).$$

Then the Gâteaux derivative in the direction of $\boldsymbol{u}$ evaluated at $\boldsymbol{w}$, denoted as $\mathcal{J}_{\boldsymbol{u}} \mathcal{G}_2[\boldsymbol{w}]$ is equal to

$$\langle \mathcal{J}_{\boldsymbol{u}} \mathcal{G}_2[\boldsymbol{w}], \boldsymbol{v} \rangle = (a(|\delta \nabla \boldsymbol{u}|) \nabla \boldsymbol{w}, \nabla \boldsymbol{v}) + \delta \left(\frac{a'(|\delta \nabla \boldsymbol{u}|)}{|\nabla \boldsymbol{u}|} [\nabla \boldsymbol{u} : \nabla \boldsymbol{w}] \nabla \boldsymbol{u}, \nabla \boldsymbol{v} \right)$$

■

We now consider the semi-discrete approximation $(\boldsymbol{u}_h, p_h) \in \boldsymbol{X}_h \times Q_h$ which solves the overall Navier-Stokes system with bounded artificial viscosity term. For notational simplicity, we drop the "h" subscripts from $\boldsymbol{u}$ and p. Define the (continuous) map $\mathcal{G} : \boldsymbol{X}_h \times Q_h \to \boldsymbol{X}_h \times Q_h$ as

$$\begin{aligned}
\langle \mathcal{G}[\boldsymbol{u}, p], (\boldsymbol{v}, q) \rangle := &(\boldsymbol{u}_t, \boldsymbol{v}) + \nu (\nabla \boldsymbol{u}, \nabla \boldsymbol{v}) + \mu \delta^{\sigma} (a(\delta |\nabla \boldsymbol{u}|) \nabla \boldsymbol{u}, \nabla \boldsymbol{v}) \\
&+ (\boldsymbol{u} \cdot \nabla \boldsymbol{u}, \boldsymbol{v}) - (p, \nabla \cdot \boldsymbol{v}) + (q, \nabla \cdot \boldsymbol{u}) - (\boldsymbol{f}, \boldsymbol{v}).
\end{aligned}$$

Therefore, we immediately have that the Gâteaux derivative of $\mathcal{G}$ in the direction of $(\boldsymbol{u}, p)$, evaluated at $(\boldsymbol{w}, r)$ is given by

$$\begin{aligned}
\left\langle \mathcal{J}_{(\boldsymbol{u},p)} \mathcal{G}[\boldsymbol{w}, r], (\boldsymbol{v}, q) \right\rangle = &(\boldsymbol{w}_t, \boldsymbol{v}) + \nu (\nabla \boldsymbol{w}, \nabla \boldsymbol{v}) + \mu \delta^{\sigma} (a(\delta |\nabla \boldsymbol{u}|) \nabla \boldsymbol{w}, \nabla \boldsymbol{v}) \\
&+ \mu \delta^{\sigma+1} \left(\frac{a'(\delta |\nabla \boldsymbol{u})}{|\nabla \boldsymbol{u}|} [\nabla \boldsymbol{u} : \nabla \boldsymbol{w}] \nabla \boldsymbol{u}, \nabla \boldsymbol{v} \right) \\
&+ (\boldsymbol{u} \cdot \nabla \boldsymbol{w}, \boldsymbol{v}) + (\boldsymbol{w} \cdot \nabla \boldsymbol{u}, \boldsymbol{v}) \\
&- (r, \nabla \cdot \boldsymbol{v}) + (q, \nabla \cdot \boldsymbol{w}) - (\boldsymbol{f}, \boldsymbol{v})
\end{aligned}$$

Now, substituting this formula for $\left\langle \mathcal{J}_{(\boldsymbol{u},p)} \mathcal{G}[\boldsymbol{w}, r], (\boldsymbol{v}, q) \right\rangle$ into the Newton iteration system

$$\left\langle \mathcal{J}_{(\boldsymbol{u}^{(n-1)}, p^{(n-1)})} \mathcal{G}[\boldsymbol{u}^{(n)} - \boldsymbol{u}^{(n-1)}, p^{(n)} - p^{(n-1)}], (\boldsymbol{v}, q) \right\rangle = - \left\langle \mathcal{G}[\boldsymbol{u}^{(n-1)}, p^{(n-1)}], (\boldsymbol{v}, q) \right\rangle,$$

we obtain the Newton iteration scheme

$$\begin{aligned}
&\left(\boldsymbol{u}_t^{(n)}, \boldsymbol{v}\right) + \nu\left(\nabla \boldsymbol{u}^{(n)}, \boldsymbol{v}\right) + \mu\delta^{\sigma}\left(a(\delta|\nabla \boldsymbol{u}^{(n-1)}|)\nabla \boldsymbol{u}^{(n)}, \nabla \boldsymbol{v}\right) \\
&+\mu\delta^{\sigma+1}\left(\frac{a'(\delta|\nabla \boldsymbol{u}^{(n-1)}|)}{|\nabla \boldsymbol{u}^{(n-1)}|}[\nabla \boldsymbol{u}^{(n-1)} : \nabla \boldsymbol{u}^{(n)}]\nabla \boldsymbol{u}^{(n-1)}, \nabla \boldsymbol{v}\right) \\
&+\left(\boldsymbol{u}^{(n-1)} \cdot \nabla \boldsymbol{u}^{(n)}, \boldsymbol{v}\right) + \left(\boldsymbol{u}^{(n)} \cdot \nabla \boldsymbol{u}^{(n-1)}, \boldsymbol{v}\right) - \left(p^{(n)}, \nabla \cdot \boldsymbol{v}\right) + \left(q, \nabla \cdot \boldsymbol{u}^{(n)}\right) \\
&\qquad = (\boldsymbol{f}, \boldsymbol{v}) + \mu\delta^{\sigma+1}\left(a'(\delta|\nabla \boldsymbol{u}^{(n-1)}|)|\nabla \boldsymbol{u}^{(n-1)}|\nabla \boldsymbol{u}^{(n-1)}, \nabla \boldsymbol{v}\right) + \left(\boldsymbol{u}^{(n-1)} \cdot \nabla \boldsymbol{u}^{(n-1)}, \boldsymbol{v}\right)
\end{aligned}$$

for all $(\boldsymbol{v}, q) \in \boldsymbol{X}_h \times Q_h$.

7. Numerical results. In this section we present numerical results for the bounded AV model (2.12)–(2.14). We start by illustrating the improvement in the bounded AV model over the overly dissipative Smagorinsky model in the numerical simulation of 2D and 3D channel flows (Section (7.1)). We then present a careful mesh refinement study supporting the error estimates (Section (7.2)).

7.1. Improvement in the BAV model. In this section, we illustrate the improvement in the bounded AV model over the overly dissipative Smagorinsky model. To this end, we have chosen the 2D and 3D channel flows.

The computational domain is $\Omega = (0, 10) \times (0, 1)$. We chose Dirichlet boundary conditions at the inlet ($x = 0$), on top ($y = 1$) and bottom ($y = 0$), and "do-nothing" boundary conditions (i.e., $(-p\mathbb{I} + 2Re^{-1}\mathbb{D}(\boldsymbol{u})) \cdot \mathbf{n} = 0$) at the outlet ($x = 10$). The boundary conditions and the forcing term have been chosen so that the exact solution be

$$\begin{aligned} u(x, y) &= 40\, y\, (1 - y) \\ v(x, y) &= 0 \\ p(x, y) &= -80\, Re^{-1}\, x \end{aligned}$$

this choice results in homogeneous boundary conditions on top and bottom, parabolic inflow profile, and the forcing term being identically zero.

We chose a large value for the horizontal velocity ($u = 10$) in the center of the channel ($y = 0.5$) since we wanted to compare the Smagorinsky model and the bounded AV model in flows displaying two regimes: (a) moderate/low velocity deformation tensors; and (b) high velocity deformation tensors. Our choice displays both regimes: the center of the channel displays regime (a) ($\|\mathbb{D}(\boldsymbol{u})\|_F = 0$) and the near-wall region displays regime (b) ($\|\mathbb{D}(\boldsymbol{u})\|_F = 80\sqrt{2}$).

We also chose $Re = 10^3$.

The numerical simulations in this section have been carried out with the Virginia Tech Large Eddy Simulator (ViTLES) (see Appendix A for a detailed description of the algorithm and computational implementation). We used a coarse nonuniform mesh of size $h = 0.5$, a small time-step $\Delta t = 10^{-4}$, and a small penalty parameter $\varepsilon = 10^{-4}$ in the penalty method to compute the pressure.

Since we use Taylor-Hood finite element spaces for the spatial discretization and Crank-Nicolson for the time-discretization, we expect that the leading term in the total error will be given by the spatial discretization for these small choices for Δt and ε ($O(h^2) \gg O(\Delta t^2) + O(\varepsilon)$). The nonlinear system at each time-step is solved with a Newton iteration up to an Euclidian norm of the residual vector less than 10^{-8}. The final time is $T = 1$ (i.e., 10^4 time-steps). Since $u = 10$ in the center of the channel, this allows a particle in the center to travel the entire length of the channel once.

It is clear that, since we have an exact solution, this flow is *not* turbulent. We chose this setting, however, because in the next section we will investigate the behavior of the error with respect to the mesh refinement (and thus we need the exact solution). Obviously, a real turbulent flow numerical comparison of the Smagorinsky and the bounded AV models is needed and will be carried out in a future study.

Figures 7.1–7.3 present numerical results for: (i) a coarse, under-resolved numerical simulation (just the NSE, without any SGS model); (ii) the Smagorinsky model (1.1); and (iii) the bounded AV model (1.2).

We chose a filter radius $\delta = 0.5$. This relatively large value for δ increased the effect of the SGS models on the numerical results, allowing a clearer comparison. We

also chose the Smagorinsky constant $C_s = 0.17$, which is a popular choice in the literature. For the bounded AV model, we chose $\mu = C_s = 0.17$ and $\sigma = 1$. These choices are identical to those for the Smagorinsky model and are most probably not optimal. The function $a(\cdot)$ was chosen to ressemble that in Figure 1:

$$a(\delta \|\mathbb{D}(\boldsymbol{u})\|_F) := -0.02 + \frac{1}{1 + 49\, e^{-5.7\,\delta\, \|\mathbb{D}(\boldsymbol{u})\|_F}} \tag{7.1}$$

This is exactly the function that was chosen in [15] for a *completely different setting* (a rotating pulse for the convection-diffusion equation). Thus, this choice is most probably not optimal for our present setting. We emphasize that we compare the Smagorinsky model with tuned parameters with the bounded AV model with nonoptimized parameters.

Figure 7.1 presents the horizontal velocity component (u) for the under-resolved (no SGS model) numerical simulation (top), the Smagorinsky model (middle), and the bounded AV model (bottom). It is clear that the under-resolved simulation yields inaccurate results. This illustrates the need for SGS modeling at this mesh resolution and Reynolds number. The Smagorinsky model yields improved results. The horizontal velocity in the center of the channel, however, is too high (11 instead of 10). The bounded AV model yields the best results. (**Integrate further in time!!!**)

The numerical results for the vertical velocity component (v) in Figure 7.2 are similar to those for u in Figure 7.1: the under-resolved simulation (top) yields poor results, the Smagorinsky model (middle) yields improved results, and the bounded AV model (bottom) yields the best results.

But the most dramatic results are those for the pressure (p) in Figure 7.3. The under-resolved simulation yields again very inaccurate results. The Smagorinsky model yields again better results, but this time the pressure gradient is about **70 times higher** than the exact value (5.5 instead of the exact value of 0.08). The bounded AV model yields much better results, the pressure gradient being reduced approximately 5 times.

This behavior is the perfect illustration of the improvement of the bounded AV model over the Smagorinsky model. Indeed, the Smagorinsky model is overly diffusive and introduces an unphysical amount of AV. Thus, the pressure gradient needs to increase dramatically to keep the same flow rate through the channel. The bounded AV model, on the other hand, introduces a moderate amount of AV which requires a much more realistic pressure gradient.

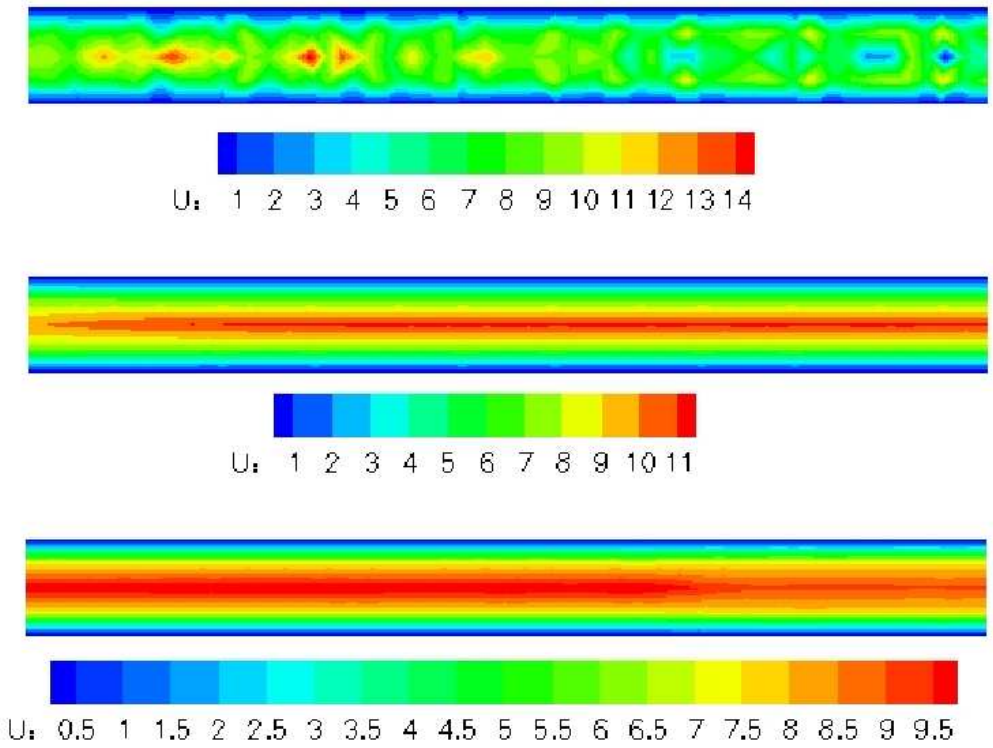

FIG. 7.1. *The horizontal velocity distribution: DNS (top); Smagorinsky (middle); and BAV (bottom).*

7.2. Mesh refinement study. In this section, we present a careful mesh refinement study supporting the error estimates in Theorem 5.1 for the bounded AV model (1.2).

7.2.1. 2D Channel Flow. To this end, we chose as a first test the same computational domain and the same boundary conditions as those in Section 7.1. This time, however, the boundary conditions and the forcing term have been chosen such that the exact solution be

$$\begin{aligned} u(x,y) &= \sin(3\,\pi\,y)\,e^{-t} \\ v(x,y) &= 0 \\ p(x,y) &= [1 - Re^{-1}\,(3\,\pi)^2]\,\sin(3\,\pi\,y)\,e^{-t}\,x \end{aligned}$$

Thus, the forcing term is identically zero, and the boundary conditions are homogeneous Dirichlet on the top and bottom of the channel, sinusoidal at the inlet, and "do-nothing" (stress-free) at the outlet. This choice of u is motivated by the vortex-Decay problem which we employ as our second numerical test.

The numerical simulations were carried out with ViTLES (see Appendix A) on 4 and 8 processors. We used a small time-step $\Delta t = 10^{-3}$ and a small penalty parameter $\varepsilon = 10^{-4}$ in our numerical experiments. Because of our discretization, as explained in the previous section, we expect the spatial discretization error to dominate the

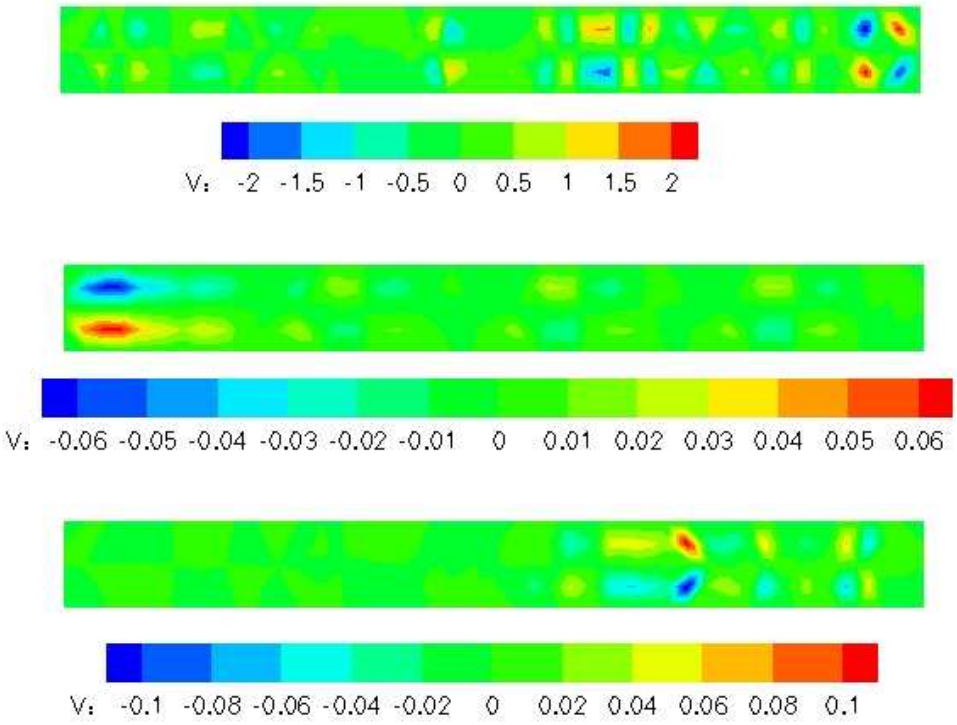

FIG. 7.2. *The vertical velocity distribution: DNS (top); Smagorinsky (middle); and BAV (bottom).*

time-discretization error. At each time-step, the Newton iteration was stopped when the Euclidian norm of the residual vector was less than 10^{-10}. We integrated the flow in time until $T = 10$, which allows a particle in the center of the channel to travel the full channel length. We chose the following parameters in the bounded AV model: the filter radius $\delta = 0.1, \mu = C_s = 0.17, \sigma = 1$, and $a(\cdot)$ the same as that in (7.1). We emphasize again that these parameters in the bounded AV model were not optimized in any way for this particular flow.

In Table 7.1, we present the $L^\infty(0,T;L^2)$ norm of the error (second column) as a function of mesh-size h (first column). We also present the observed order of accuracy (third column) and the theoretical order of accuracy given by Theorem 5.1 (fourth column). (**More to follow...**)

TABLE 7.1
Taylor Hood finite element discretization, $\|e\|_{L^\infty(0,T;L^2)}$.

h	$\|e\|_{L^\infty(0,T;L^2)}$	Observed Order of Accuracy	Theoretical Order of Accuracy
1/2	0.1		2
1/4	0.01	2.2	2

7.2.2. The 2D Vortex Decay Problem. In this section, we present numerical results for the bounded AV model applied to the vortex decay problem of Chorin [7]. A similar study for the vortex decay problem using the Smagorinsky model was presented

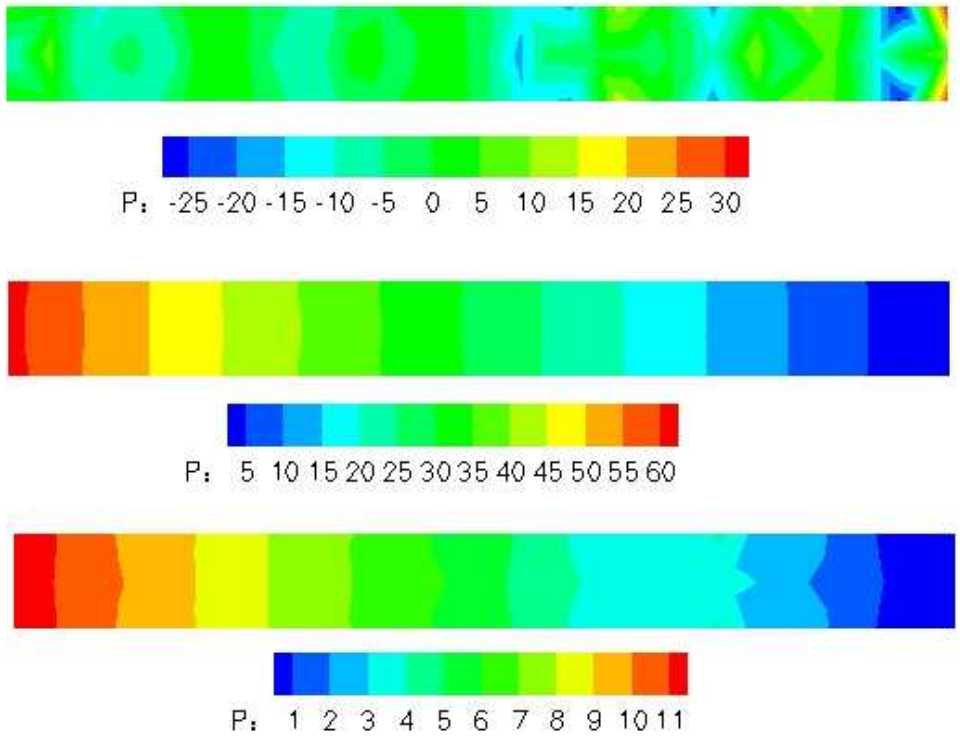

FIG. 7.3. *The pressure distribution: DNS (top); Smagorinsky (middle); and BAV (bottom).*

in [17]. For the vortex decay problem, we define the domain $\Omega = (0,1)^2 \subset \mathbf{R}^2$, and specify

$$\begin{aligned} u_1 &:= -\cos(n\pi x)\sin(n\pi y)\exp(-2n^2\pi^2 t/\tau), \\ u_2 &:= \sin(n\pi x)\cos(n\pi y)\exp(-2n^2\pi^2 t/\tau), \\ p &:= -\frac{1}{4}(\cos(2n\pi x) + \cos(2n\pi y))\exp(-4n^2\pi^2 t/\tau). \end{aligned}$$

Note that for $\tau := \mathrm{Re}^{-1}$, the set (u_1, u_2, p) solves the time-dependent Navier-Stokes equations with the appropriate (time dependent, Dirichlet) boundary conditions. For our purposes, we take (7.2) as the solution to (**??**) and illustrate two points: that the spatial semi-discretization error estimates are satisfied and that the estimates are bounded uniformly with respect to the Reynolds number.

Accordingly, we specify the following parameters,

$$\begin{aligned} \mathrm{Re} &:= 10^{10}, \\ \tau &:= 1000, \\ \text{final time } T &:= 2, \\ \text{eddy scale } \delta &:= 0.1, \\ \mu = C_s^2 &:= 0.17^2, \\ \Delta t &:= 0.01. \end{aligned}$$

h	$\|u-u_h\|_{L^\infty(0,T;L^2)}$	rate	$\|u-u_h\|_{L^2(0,T;L^2)}$	rate	$\|u-u_h\|_{L^2(0,T;H^1)}$	rate
1/8	$4.020927 \cdot 10^{-1}$		$4.936365 \cdot 10^{-1}$		$1.560773 \cdot 10^{1}$	
1/16	$3.103567 \cdot 10^{-2}$	3.70	$3.952673 \cdot 10^{-2}$	3.64	$2.886625 \cdot 10^{0}$	2.43
1/24	$5.534371 \cdot 10^{-3}$	4.25	$7.594030 \cdot 10^{-3}$	4.07	$1.096755 \cdot 10^{0}$	2.39
1/32	$1.822532 \cdot 10^{-3}$	3.86	$2.418206 \cdot 10^{-3}$	3.98	$5.182457 \cdot 10^{-1}$	2.61
1/40	$7.778230 \cdot 10^{-4}$	3.82	$1.018835 \cdot 10^{-3}$	3.87	$2.870239 \cdot 10^{-1}$	2.65
1/48	$4.227375 \cdot 10^{-4}$	3.34	$5.138958 \cdot 10^{-4}$	3.75	$1.763596 \cdot 10^{-1}$	2.68
1/56	$2.567581 \cdot 10^{-4}$	3.26	$2.907396 \cdot 10^{-4}$	3.70	$1.166515 \cdot 10^{-1}$	2.68
1/64	$1.645877 \cdot 10^{-4}$	3.33	$1.779283 \cdot 10^{-4}$	3.68	$8.151033 \cdot 10^{-2}$	2.68
1/72	$1.102856 \cdot 10^{-4}$	3.40	$1.154125 \cdot 10^{-4}$	3.68	$5.940966 \cdot 10^{-2}$	2.69

TABLE 7.2
Finite element convergence estimates for the vortex decay problem.

For our calculations, we assume $n = 3$, i.e. a 3×3 array of vortices and study the finite element convergence rates for fixed $\delta := 0.1$ as $h \to 0$. For the spatial discretization, we take the Taylor-Hood finite element pair and implement the Newton iteration scheme as described in Section 6. For the temporal discretization, we use the Crank-Nicholson scheme. Indicated in Table 7.2, the spatial semi-discretization convergence estimates follow their predicted values of 3 in the spatial L^2 norm and 2 in the spatial H^1 norm. Also, note that these estimates are *independent* of the selected Reynolds number, as we have taken a relatively high value for Re and a relatively high value for Δt.

Acknowledgments. The authors thank .....

Appendix A. The Virginia Tech Large Eddy Simulator (ViTLES).

We introduce in this paper *ViTLES*, the Virginia Tech Large Eddy Simulator, a *parallel, finite element* computational platform for the numerical validation and testing of new LES approaches. We describe next the numerical algorithm and its computational implementation.

A.1. Algorithm: Spatial Discretization. For spatial discretization, we use the finite element (FE) method with the usual Galerkin formulation.

The computational domain is decomposed in a collection of non-overlapping triangles (in 2D) or tetrahedra (in 3D). Thus, the geometric flexibility of FE allows us to treat complex geometries.

We use Taylor-Hood finite elements: on each triangle (2D) or tetrahedron (3D), each velocity component is a quadratic polynomial, and the pressure is a liniar polynomial. The basis functions for the velocity are defined at vertices and the midpoints of the edges; the basis functions for the pressure are defined at the vertices.

From the choice of nodal points, both velocity and pressure are continuous across the element (triangle or tetrahedron) boundaries (Cuvelier et al. [8], p. 238). One can also show that the Taylor-Hood finite elements satisfy the inf-sup (or Ladyzhenskaya-Babuska-Brezzi) condition (see Brenner and Scott [6], p. 253-255).

A.2. Algorithm: Time Discretization. For time discretization, we used Crank-Nicolson. This is an implicit method, second order accurate in time. It is also A-stable (see Cuvelier et al. [8], p. 330-333). Since the Crank-Nicolson method is implicit in time, one needs to pay a higher computational cost by solving a nonlinear system of equations at each time step. The payoff is the increased stability of the calculation, which is very impotant in the numerical simulation of turbulent flows.

Thus, at each time step, one has to solve

$$\begin{aligned} &\frac{\boldsymbol{u}^{k+1}-\boldsymbol{u}^{k}}{\Delta t} - \theta\nabla\cdot\left(2\mu\mathbb{D}(\boldsymbol{u}^{k+1})\right) + \theta(\boldsymbol{u}^{k+1}\cdot\nabla)\boldsymbol{u}^{k+1} + \theta\nabla p^{k+1} \qquad \text{(A.1)}\\ &= (1-\theta)\nabla\cdot\left(2\mu\mathbb{D}(\boldsymbol{u}^{k})\right) - (1-\theta)(\boldsymbol{u}^{k}\cdot\nabla)\boldsymbol{u}^{k} - (1-\theta)\nabla p^{k} + \theta\mathbf{f}^{k+1} + (1-\theta)\mathbf{f}^{k}, \end{aligned}$$

where $(\boldsymbol{u}^{k+1}, p^{k+1}, \mathbf{f}^{k+1})$ and $(\boldsymbol{u}^{k}, p^{k}, \mathbf{f}^{k})$ are the velocity, pressure, and forcing vectors at the current and previous time-step, respectively, $\theta = \frac{1}{2}$ for Crank-Nicolson, and Δt is the time-step. We use Newton's method to solve the resulting nonlinear system in (A.1); a detailed description of our approach is presented in section A.4.

A.3. Algorithm: Penalty Method. The incompressibility constraint $\nabla\cdot\boldsymbol{u} = 0$ in the Navier-Stokes equations (2.1)–(2.3) is relaxed through the penalty method:

$$\varepsilon p_\varepsilon + \nabla\cdot\boldsymbol{u}_\varepsilon = 0, \qquad \text{(A.2)}$$

where ε is a small parameter. This popular approach is described in Cuvelier et al. [8] (Chapter 8 and Section 10.3.1), in Gunzburger [13] (Chapter 5 and Section 7.1), and in Quarteroni and Valli [26] (Section 9.6.4).

Obviously, the incompressibility constraint is no longer satisfied, but it can be proven that (formula (5.16) in [13])

$$|\boldsymbol{u} - \boldsymbol{u}_\varepsilon|_1 + ||p - p_\varepsilon||_0 \leq C\,\varepsilon.$$

Thus, as $\varepsilon \to 0$, the solution of the penalized problem converges to that of the unpenalized problem. In our computations. we used $\varepsilon = 0.0001$.

A.4. Algorithm: Newton Iteration. Since we are using an implicit method for time discretization (Crank-Nicolson), we need to solve a nonlinear system of equations at each time step. To do this, we use Newton's Method because of its fast (quadratic) convergence. Before describing Newton's Method for our setting, we need to comment on the incompressibility constraint.

As mentioned in the previous subsection, we use the penalty method (A.2) to perturb the incompressibility constraint. The time discretization we chose for the penalty method reads

$$\varepsilon p^{k+1} + \nabla \cdot \boldsymbol{u}^{k+1} = \varepsilon p^k,$$

where the $k+1$ superscript denotes the current time step, and the k superscript denotes the previous time step. In this form, the penalty method ressembles the artificial compressibility method described in Gunzburger [13] p.77, Cuvelier et al. [8] p. 339-340, the Augmented Lagrangian method described in Quarteroni and Valli [26] p. 330, or the Iterated Penalty method described in Gunzburger [13] p. 76. It is interesting to note that the Iterated Penalty method for stationary Navier-Stokes equations satisfies

$$|\boldsymbol{u} - \boldsymbol{u}^{(n)}|_1 + ||p - p^{(n)}||_0 = O(\varepsilon^n),$$

where n is the number of iterations. Thus, it seems natural to expect more than linear convergence for our time-dependent formulation for the penalty method (A.2); further investigation is needed.

Putting together (A.1) and (A.2), at each time-step we have to solve

$$R(\boldsymbol{u}^{k+1}, p^{k+1}) = \boldsymbol{0}$$

where

$$\begin{aligned} R(\boldsymbol{u}^{k+1}, p^{k+1}) := (&\boldsymbol{u}^{k+1} - \theta\Delta t\nabla \cdot (2\mu\mathbb{D}(\boldsymbol{u}^{k+1})) + \theta\Delta t(\boldsymbol{u}^{k+1} \cdot \nabla)\boldsymbol{u}^{k+1} + \theta\Delta t\nabla p^{k+1} + R_k, \\ &\nabla \cdot \boldsymbol{u}^{k+1} + \varepsilon p^{k+1} - \varepsilon p^k) \end{aligned} \tag{A.3}$$

and R_k is the part of $R(\boldsymbol{u}^{k+1}, p^{k+1})$ that depends only on $\boldsymbol{u}^k$ and p^k:

$$R_k := -\boldsymbol{u}^k - (1-\theta)\Delta t\nabla \cdot (2\mu\mathbb{D}(\boldsymbol{u}^k)) + (1-\theta)\Delta t(\boldsymbol{u}^k \cdot \nabla)\boldsymbol{u}^k + (1-\theta)\Delta t\nabla p^k.$$

The Newton iteration $(\boldsymbol{u}^n, p^n)$ will yield an approximation to $(\boldsymbol{u}^{k+1}, p^{k+1})$, where n is the Newton iteration number. We choose to start the Newton iteration with the velocity and pressure obtained at the previous time-step:

$$\boldsymbol{u}^0 = \boldsymbol{u}^k \qquad \text{and} \qquad p^0 = p^k.$$

Thus, we need to solve

$$R(\boldsymbol{u}^n, p^n) = \boldsymbol{0}.$$

Newton's method now reads

$$R'(\boldsymbol{u}^n, p^n)(\boldsymbol{u}^{n+1} - \boldsymbol{u}^n, p^{n+1} - p^n) = -R(\boldsymbol{u}^n, p^n),$$

where

$$[R'(\boldsymbol{u}^n, p^n)]_{ij} := \frac{\partial R_i(\boldsymbol{u}^n, p^n)}{\partial(\boldsymbol{u}^n, p^n)_j}$$

is the Jacobian of R. We explicitly construct the approximation to R', element by element, from a sequence of finite differences

$$[R'(\boldsymbol{u}^n, p^n)]_{ij} \approx \frac{R_i((\boldsymbol{u}^n, p^n) + h\mathbf{e}_j) - R_i((\boldsymbol{u}^n, p^n)}{h},$$

where h is the differencing parameter and $\mathbf{e}_j$ is the j-th unit vector. The reason for using an explicit construction of the approximation to the Jacobian instead of using matrix-free Jacobian vector products is that we will need the actual Jacobian matrix in sensitivity computations in our longer-term research. We also note that our finite difference implemenatation for the Jacobian is ripe for automatic differentiation.

A.5. Computational Implementation. ViTLES is written on top of PETSc (the portable, extensible toolkit for scientific computing) developed at Argonne National Laboratory [2, 1, 3]. It makes use of MPI, linpack and the blas. We have also used ADIC, the automatic differentiation tool [14], to compute Jacobians. This allows us to rapidly implement different boundary condition and closure models as well as perform sensitivity analysis. Routines have been developed to convert ViTLES format to several visualization routines including Tecplot, VTK and VU.

REFERENCES

[1] Satish Balay, Kris Buschelman, Victor Eijkhout, William D. Gropp, Dinesh Kaushik, Matthew G. Knepley, Lois Curfman McInnes, Barry F. Smith, and Hong Zhang, *PETSc users manual*, Tech. Report ANL-95/11 - Revision 2.1.5, Argonne National Laboratory, 2004.

[2] Satish Balay, Kris Buschelman, William D. Gropp, Dinesh Kaushik, Matthew G. Knepley, Lois Curfman McInnes, Barry F. Smith, and Hong Zhang, *PETSc Web page*, 2001, http://www.mcs.anl.gov/petsc.

[3] Satish Balay, Victor Eijkhout, William D. Gropp, Lois Curfman McInnes, and Barry F. Smith, *Efficient management of parallelism in object oriented numerical software libraries*, Modern Software Tools in Scientific Computing (E. Arge, A. M. Bruaset, and H. P. Langtangen, eds.), Birkhäuser Press, 1997, pp. 163–202.

[4] L.C. Berselli, T. Iliescu, and W.J. Layton, *Mathematics of large eddy simulation of turbulent flows*, Springer Verlag, 2005.

[5] J. Boussinesq, *Essai sur la théorie des eaux courantes,*, Mém. prés par div. savants á la Acad. Sci. **23** (1877), 1–680.

[6] Susanne C. Brenner and L. Ridgway Scott, *The mathematical theory of finite element methods*, Texts in Applied Mathematics, vol. 15, Springer-Verlag, New York, 1994. MR MR1278258 (95f:65001)

[7] Alexandre Joel Chorin, *Numerical solution of the Navier-Stokes equations*, Math. Comp. **22** (1968), 745–762. MR MR0242392 (39 #3723)

[8] C. Cuvelier, A. Segal, and A. A. van Steenhoven, *Finite element methods and Navier-Stokes equations*, Mathematics and its Applications, vol. 22, D. Reidel Publishing Co., Dordrecht, 1986. MR MR850259 (88g:65106)

[9] Qiang Du and Max D. Gunzburger, *Finite-element approximations of a Ladyzhenskaya model for stationary incompressible viscous flow*, SIAM J. Numer. Anal. **27** (1990), no. 1, 1–19. MR MR1034917 (91e:65123)

[10] ———, *Analysis of a Ladyzhenskaya model for incompressible viscous flow*, J. Math. Anal. Appl. **155** (1991), no. 1, 21–45. MR MR1089323 (92e:35134)

[11] U. Frisch, *Turbulence, the Legacy of A.N. Kolmogorov*, Cambridge University Press, Cambridge, 1995.

[12] M. Germano, U. Piomelli, P. Moin, and W.H. Cabot, *A dynamic subgrid-scale eddy viscosity model*, Phys. Fluids A **3** (1991), 1760–1765.

[13] Max D. Gunzburger, *Finite element methods for viscous incompressible flows*, Computer Science and Scientific Computing, Academic Press Inc., Boston, MA, 1989, A guide to theory, practice, and algorithms. MR MR1017032 (91d:76053)

[14] Paul Hovland, Boyana Norris, and Christian Bischof, *ADIC Web page*, 2005, http://www-fp.mcs.anl.gov/adic/.

[15] T. Iliescu, *Genuinely nonlinear models for convection-dominated problems*, Comput. Math. Appl. **48** (2004), no. 10-11, 1677–1692. MR MR2107123 (2005h:76064)
[16] V. John, *Large eddy simulation of turbulent incompressible flows*, Lecture Notes in Computational Science and Engineering, vol. 34, Springer-Verlag, Berlin, 2004, Analytical and numerical results for a class of LES models. MR 2 018 955
[17] V. John and W. J. Layton, *Analysis of numerical errors in large eddy simulation*, SIAM J. Numer. Anal. **40** (2002), no. 3, 995–1020 (electronic). MR MR1949402 (2004i:76132)
[18] O.A. Ladyžhenskaya, *New equations for the description of motion of viscous incompressible fluids and solvability in the large of boundary value problems for them*, Proc. Steklov Inst. Math. **102** (1967), 95–118.
[19] O.A. Ladyžhenskaya, *Modifications of the Navier-Stokes equations for large gradients of the velocities*, Zap. Naučn. Sem. Leningrad. Otdel. Mat. Inst. Steklov. (LOMI) **7** (1968), 126–154. MR 39 #3169
[20] William J. Layton, *A nonlinear, subgridscale model for incompressible viscous flow problems*, SIAM J. Sci. Comput. **17** (1996), no. 2, 347–357. MR MR1374284 (96k:76073)
[21] D.K. Lilly, *The representation of small scale turbulence in numerical simulation experiments*, Proc. IBM Sci. Computing Symp. On Environmental Sciences (Yorktown Heights, NY) (H.H. Goldstine, ed.), 1967, pp. 195–210.
[22] C. Meneveau, T. Lund, and W. Cabot, *A lagrangian dynamic subgrid-scale model of turbulence*, J. Fluid Mech. **319** (1996), 353–385.
[23] U. Piomelli, W.H. Cabot, P. Moin, and S. Lee, *Subgrid-scale backscatter in turbulent and transitional flow*, Phys. Fluids **3** (1991), no. 7, 1766–1771.
[24] S.B. Pope, *Turbulent flows*, Cambridge University Press, Cambridge, 2000. MR 2003f:76002
[25] F. Porté-Agel, C. Meneveau, and M. B. Parlange, *A scale-dependent dynamic model for large-eddy simulation: application to a neutral atmospheric boundary layer*, J. Fluid Mech. **415** (2000), 261–284. MR MR1775927 (2001e:76074)
[26] Alfio Quarteroni and Alberto Valli, *Numerical approximation of partial differential equations*, Springer Series in Computational Mathematics, vol. 23, Springer-Verlag, Berlin, 1994. MR MR1299729 (95i:65005)
[27] L.F. Richardson, *Weather prediction by numerical process*, Cambridge University Press, Cambridge, 1922.
[28] P. Sagaut, *Large eddy simulation for incompressible flows*, Scientific Computation, Springer-Verlag, Berlin, 2001, An introduction, With an introduction by Marcel Lesieur, Translated from the 1998 French original by the author. MR 2002f:76047
[29] J.S. Smagorinsky, *General circulation experiments with the primitive equations*, Mon. Weather Review **91** (1963), 99–164.
[30] E.R. van Driest, *On turbulent flow near a wall*, J. Aerospace Sci. **23** (1956), 1007–1011.
[31] J. von Neumann and R.D. Richtmyer, *A method for the numerical calculation of hydrodynamic shocks*, J. Appl. Phys. **21** (1950), 232–237.